Quantitative Characterisation of SiPM Radiation Damage using Emission Microscopy

Projet de master en physique - PHYS-599(b)

Presenter: Lai Gui

Supervisors: Dr Esteban Currás Rivera, Dr Guido Haefeli
Responsible Professor: Prof. Olivier Schneider

Outline

- **Introduction**: LHC, LHCb Upgrade II, and working principle of SiPM
- **Methodology**: DCR, secondary photon emission, and the EMMI technique
- **Experimental Procedures**: sensors, V_{bd} extraction, and the analysis pipeline
- **Results**: extracted damage metrics
- **Conclusion and Outlook**

The LHC and LHCb

- **LHC**: 27 km pp collider, $\sqrt{s}$ = 13.6 TeV (Run 3), 2 counter-rotating beams with 4 interaction points
- **LHCb**: single-arm forward spectrometer in b- and c-hadron physics, CP violation, rare decays
- **SciFi Tracker**: sits downstream of the dipole magnet and is read out by SiPMs
- **LHCb Upgrade II**: ~5× integrated luminosity → ~5× radiation fluence on detectors

European Southern Observatory (ESO).
Aerial view of the CERN site near Geneva.
[Online; accessed 25-June-2026]. 2026.

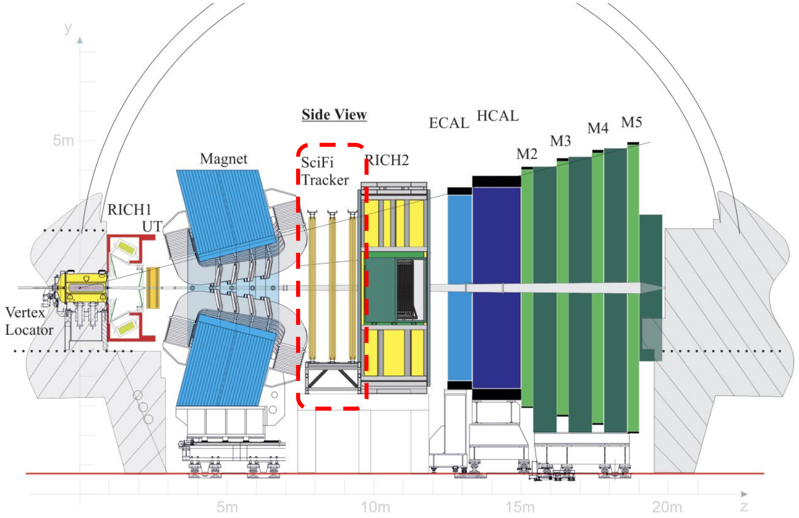

LHCb Collaboration. LHCb Tracker Upgrade Technical Design Report. Tech. rep. 2014. doi: 10.17181/CERN.OOOE.9O9T.

Radiation at the LHCb Upgrade II

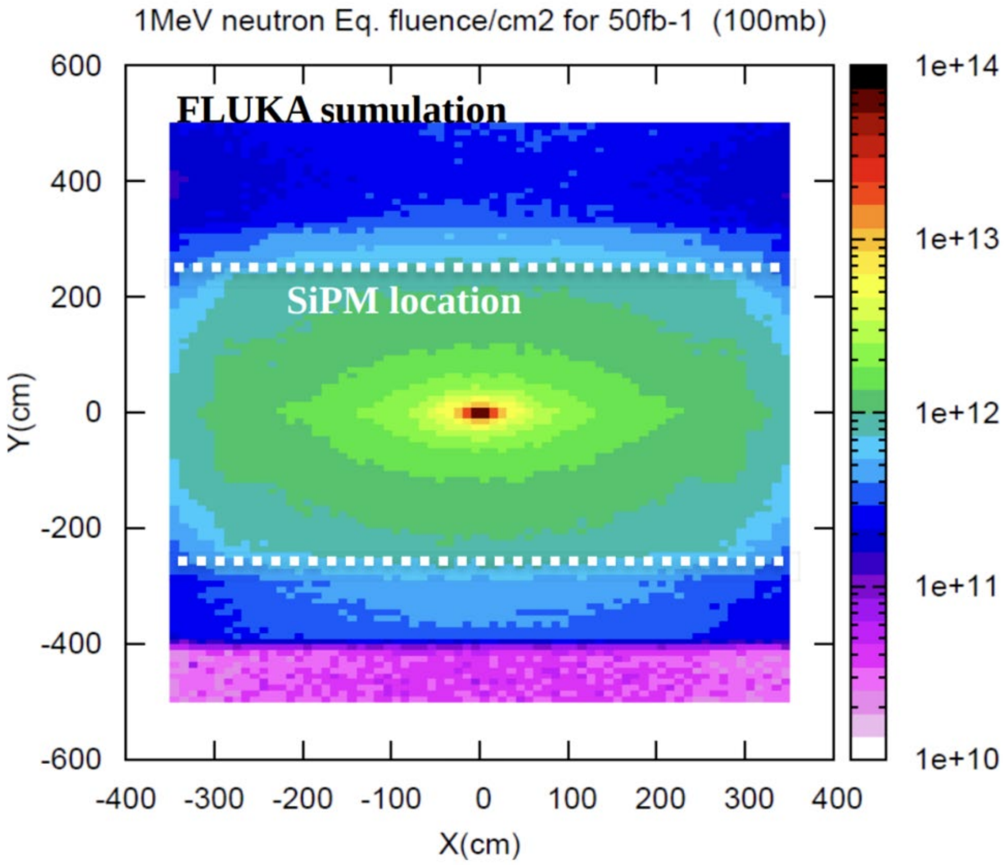

Simulated 1-MeV-neq fluence in LHCb after full HL-LHC operation
LHCb Collaboration. LHCb Tracker Upgrade Technical Design Report. Tech. rep. 2014. doi: 10.17181/CERN.OOOE.9O9T.

- **FLUKA simulation**: SciFi SiPMs are off-axis, reduced but still significant neutron flux
- **Expected fluence**: ~3×10^{12} n_{eq}/cm^2 over the LHCb Upgrade II operation period
- **This work**: characterises damage up to 1×10^{13} n_{eq}/cm^2 (a 3× safety margin)
- **Goal**: develop tool for radiation damage characterisation in aid for developing radiation-tolerant SiPM technology

How a SiPM Works

- Array of SPAD microcells in Geiger mode: $V_{bias} > V_{bd}$
  - Overvoltage $OV = V_{bias} - V_{bd}$ sets gain & trigger probability
- Single carrier could produce self-sustaining avalanche, leading to measurable current even with single photon
- Quenching resistor stops avalanche;
  recovery time $\tau_{rec} = R_q \cdot C_{cell}$
- Summed output is proportional to number of cells fired, which allows photon counting
- Compared to PMTs, SiPMs achieve higher granularity, insensitive to B-field, however vulnerable to radiation damage

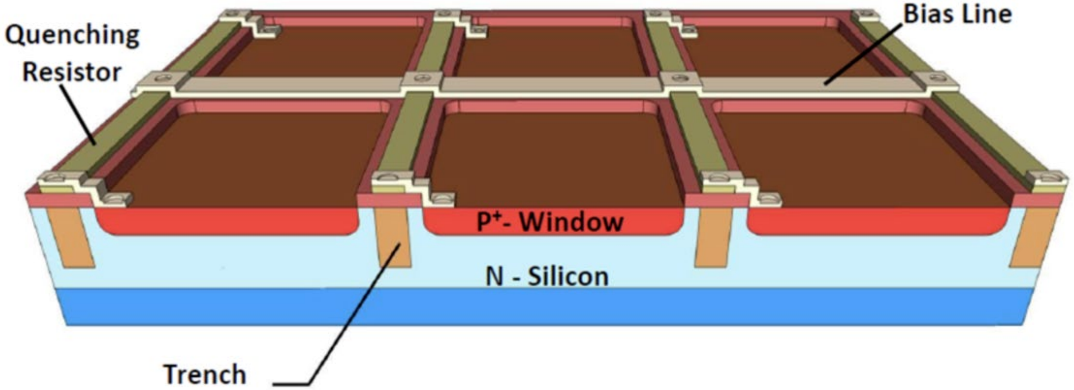

S. Vinogradov. “The Silicon Photomultiplier (SiPM) Concept and Design Development”. In: APPEC News (Mar. 2015).

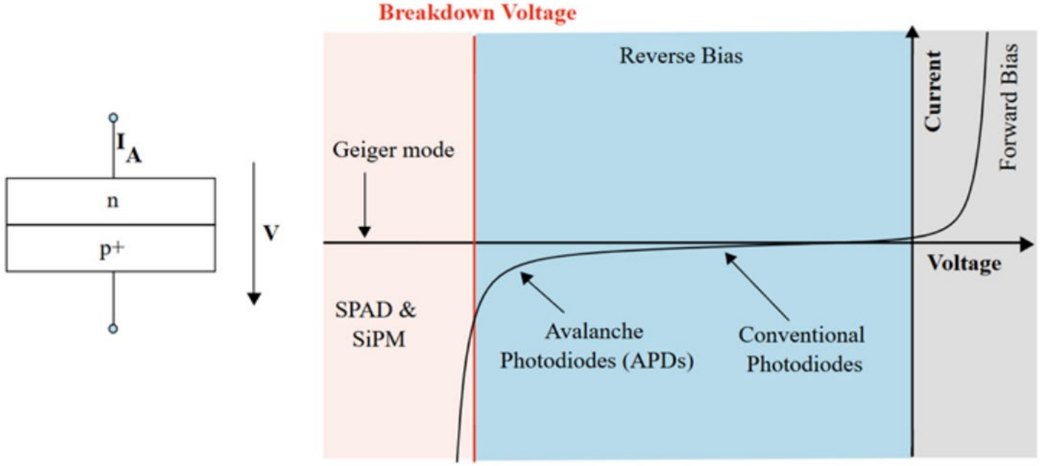

Single-Photon Avalanche Diode (SPADs). MeetOptics Academy.

Dark Count Rate — the Damage Proxy

- Lattice defects leads to mid-gap states that allows Shockley–Read–Hall generation (two-step “stepping stones”)
- Thermal carrier in high-field region triggers avalanche, which are indistinguishable from a photon count
- DCR is related to defect density and is an indicator of the accumulated neutron fluence
- **Spatial map of dark-count activity = map of radiation damage**

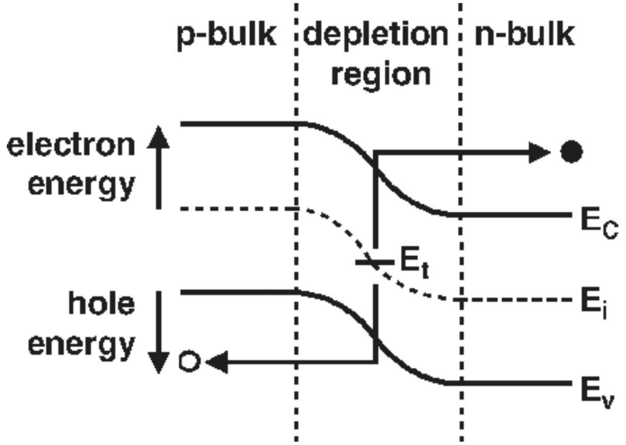

A.J. Scholten. “The physical background of JUNGAP2”. October 2006. DOI:10.1109/TED.2005.881004

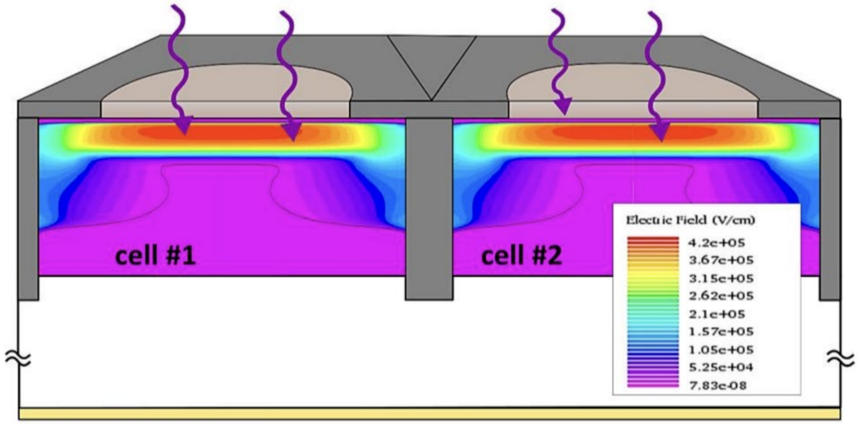

F. Acerbi. SiPM rad-hard R&D: AIDAinnova production at FBK. Presentation at Fondazione Bruno Kessler (FBK). Presented on 2025-05-14. May 2025.

Secondary Photon Emission

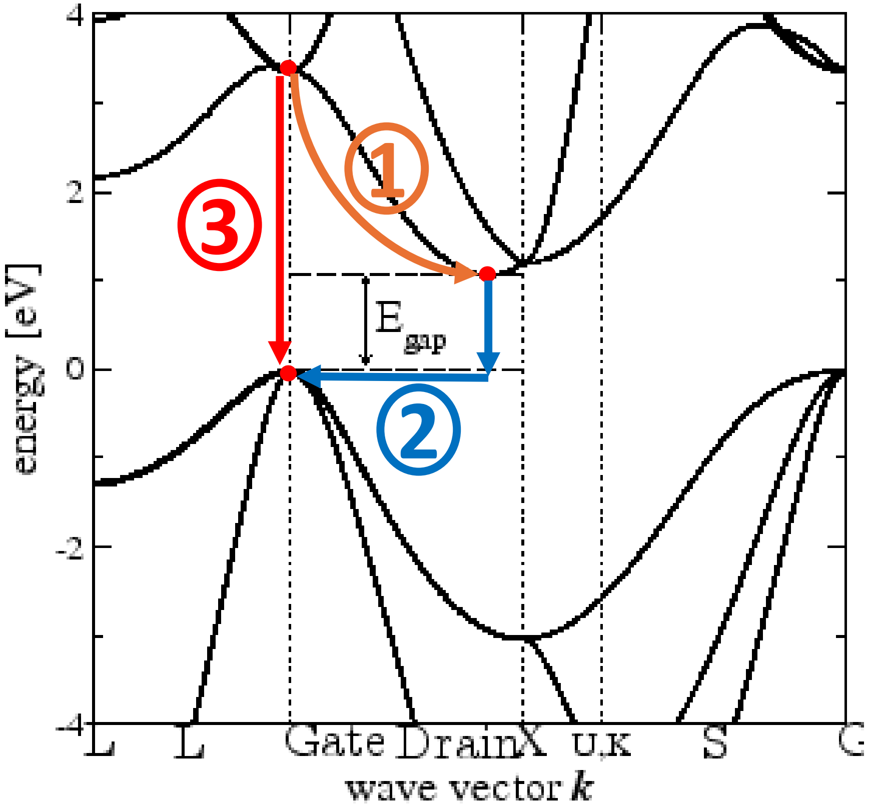

S.-E. Ungersböck. "Advanced Modeling of Strained CMOS Technology". PhD thesis. Institute for Microelectronics, TU Wien, 2007.

- Hot carriers in the avalanche emit faint light:
  ~1 photon per 10^5–10^6 carriers

  (1) **Intraband bremsstrahlung** → broad visible-IR continuum (~500–1600 nm)

  (2) **Indirect interband transition** → near-IR ~1100–1200 nm

  (3) **Direct interband transition** → UV ~365 nm, mostly reabsorbed in Si

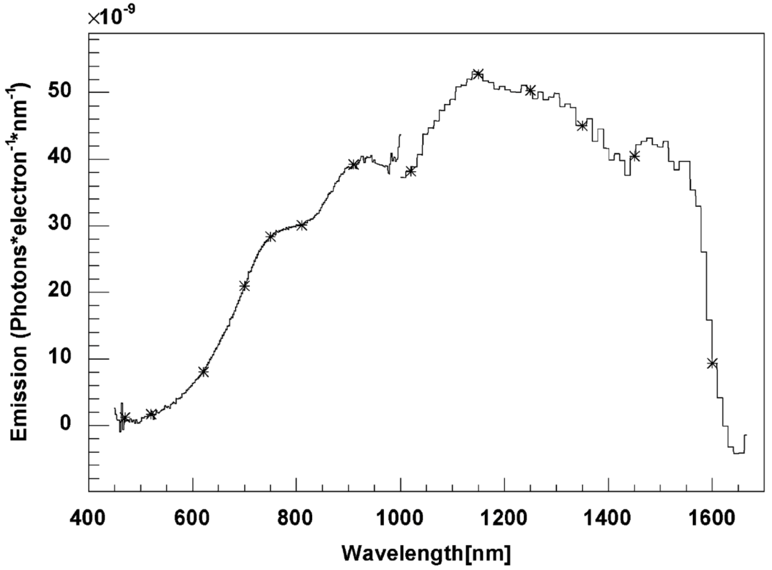

R. Mirzoyan. "Light emission in Si avalanches". 27 May 2009. doi:10.1016/j.nima.2009.05.081

- Photon emission = hot carrier generation → dark-count activity

Experimental Setup

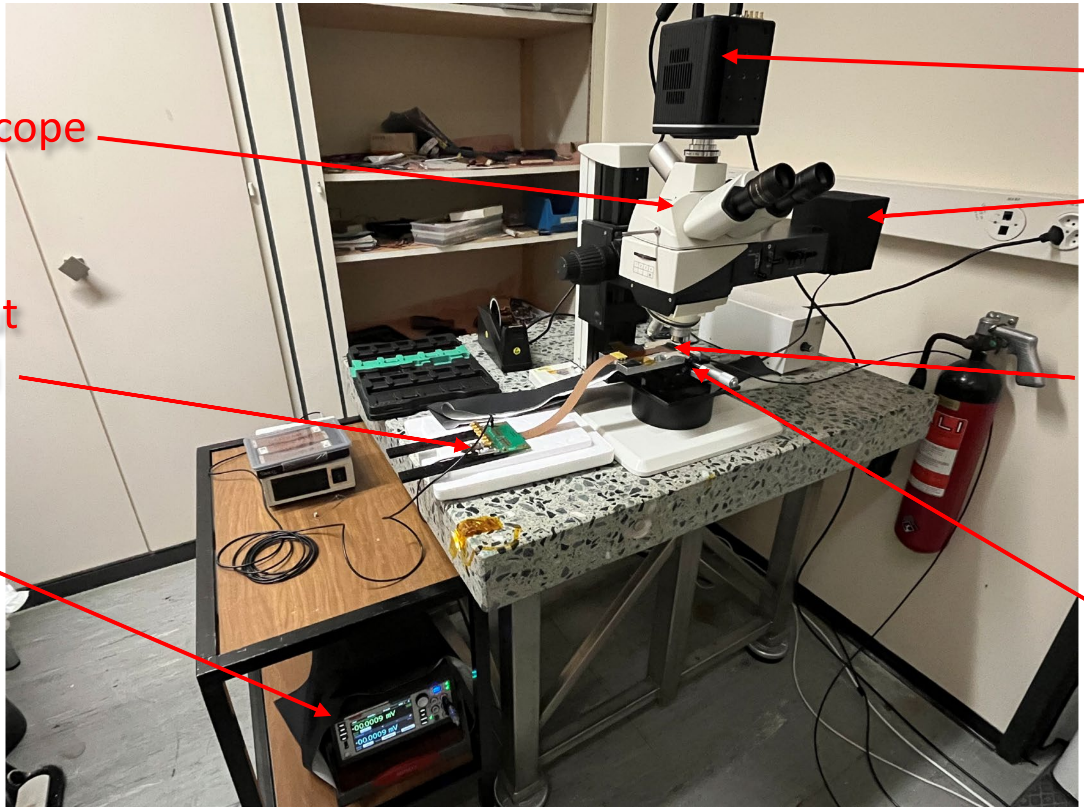

EMMI bench, dark room (Cubotron)

- Hamamatsu ORCA-Quest 2 qCMOS, −20 °C, 16-bit, 4096×2304 px
- Leica microscope (5x/20x/50x), with a light source for focus adjustment and reference image taking
- Keithley 2450 SMU: bias + current logged every 5 s
- Black-cloth covering against light in the dark room

Emission Microscopy (EMMI)

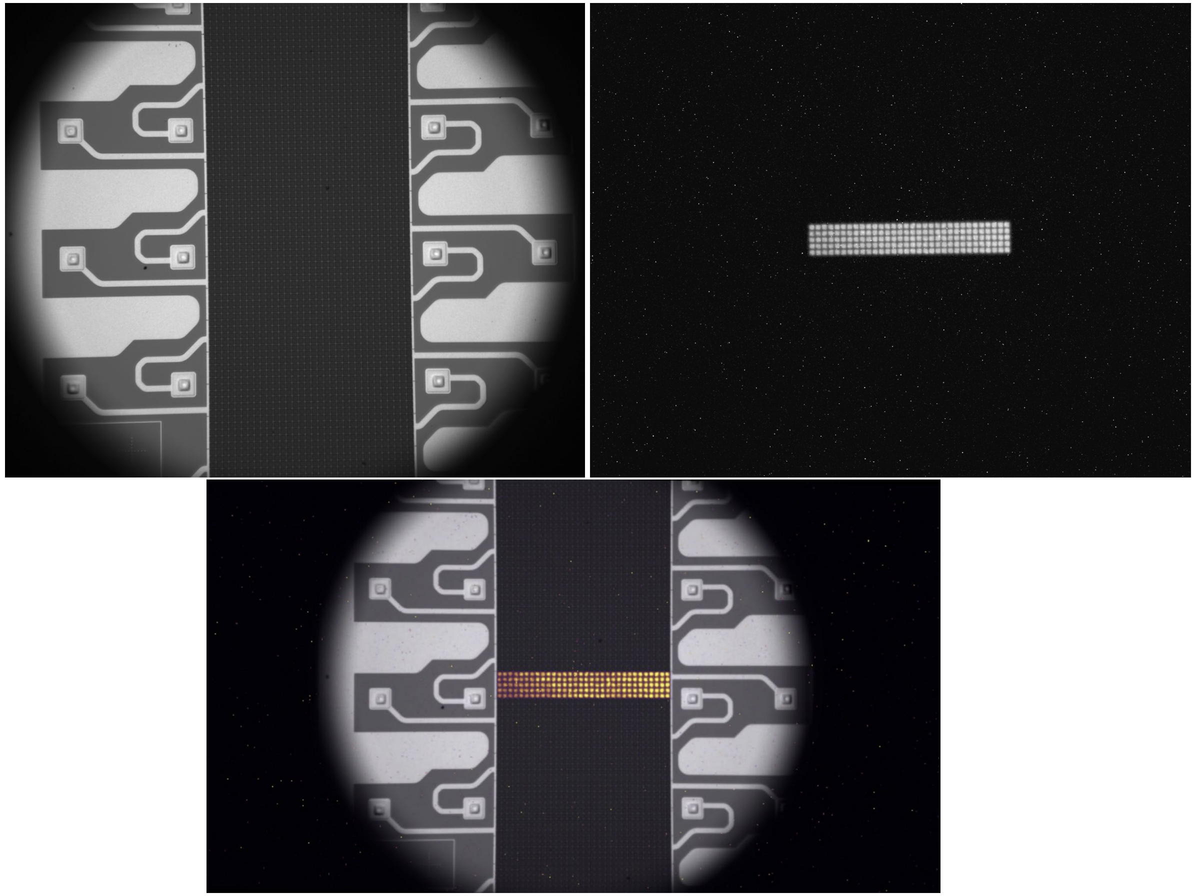

Reference image (top left), emission image (top right), and the combined EMMI image (bottom)

- Mature integrated-circuit failure analysis technique (1990s) transferred to SiPM damage mapping
- Reference image: ~3 ms, illuminated → cell structure
- Emission image: 10 min in the dark → secondary photons from avalanches
- Superposition with alpha-coupled colormap to illustrate emission localised within each cell

Sensors Under Test (Hamamatsu)

Producer	Name	Pixel Size	Fluence	V_{bd} (ch118)
Hamamatsu	H2024	50um	1e13 n_{eq}/cm^2	51.69 ± 0.02 V
	H2024	50um	3e12 n_{eq}/cm^2	50.97 ± 0.02 V
	H2024	50um	1e12 n_{eq}/cm^2	51.45 ± 0.07 V
	H2024	50um	3e11 n_{eq}/cm^2	51.31 ± 0.02 V
	H2024	50um	0 n_{eq}/cm^2	51.10 ± 0.11 V

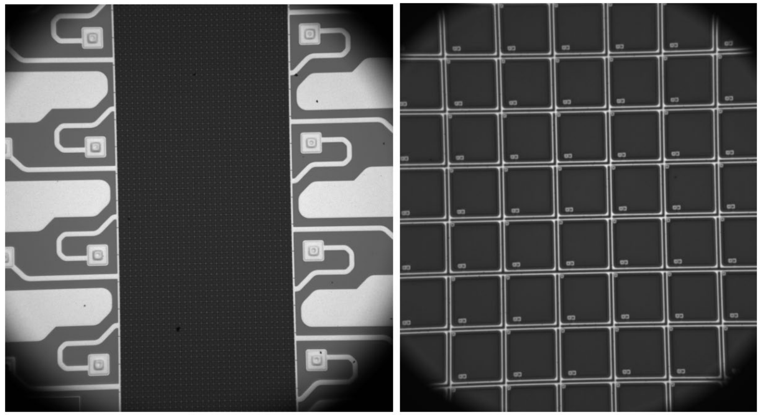

Hamamatsu H2024 — 50 μm pitch, $V_{bd} \approx 51$ V

Producer	Name	Pixel Size	Fluence	V_{bd} (ch118)
FBK	W3m	31um	1e13 n_{eq}/cm^2	31.07 ± 0.02 V
	W3m	31um	3e12 n_{eq}/cm^2	31.00 ± 0.02 V
	W3m	31um	1e12 n_{eq}/cm^2	31.11 ± 0.02 V
	W3m	31um	3e11 n_{eq}/cm^2	31.19 ± 0.02 V
	W1m	31um	0 n_{eq}/cm^2	30.94 ± 0.04 V

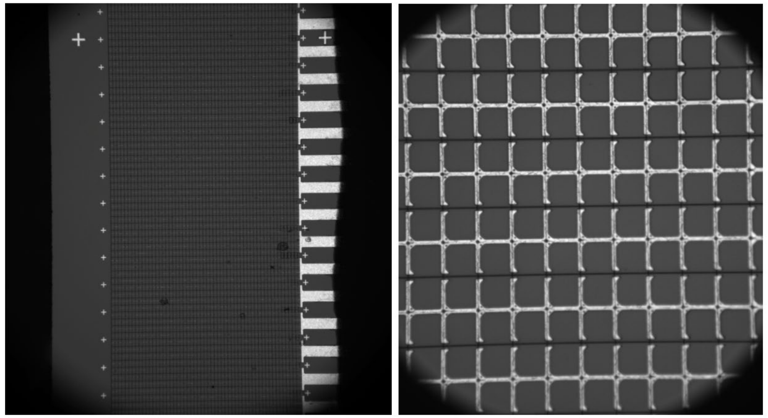

FBK W3m — 31 μm pitch, $V_{bd} \approx 31$ V

- V_{bd} stable, consistent with the assumption of no variation across different fluences

Breakdown Voltage — ILD Method

EPFL

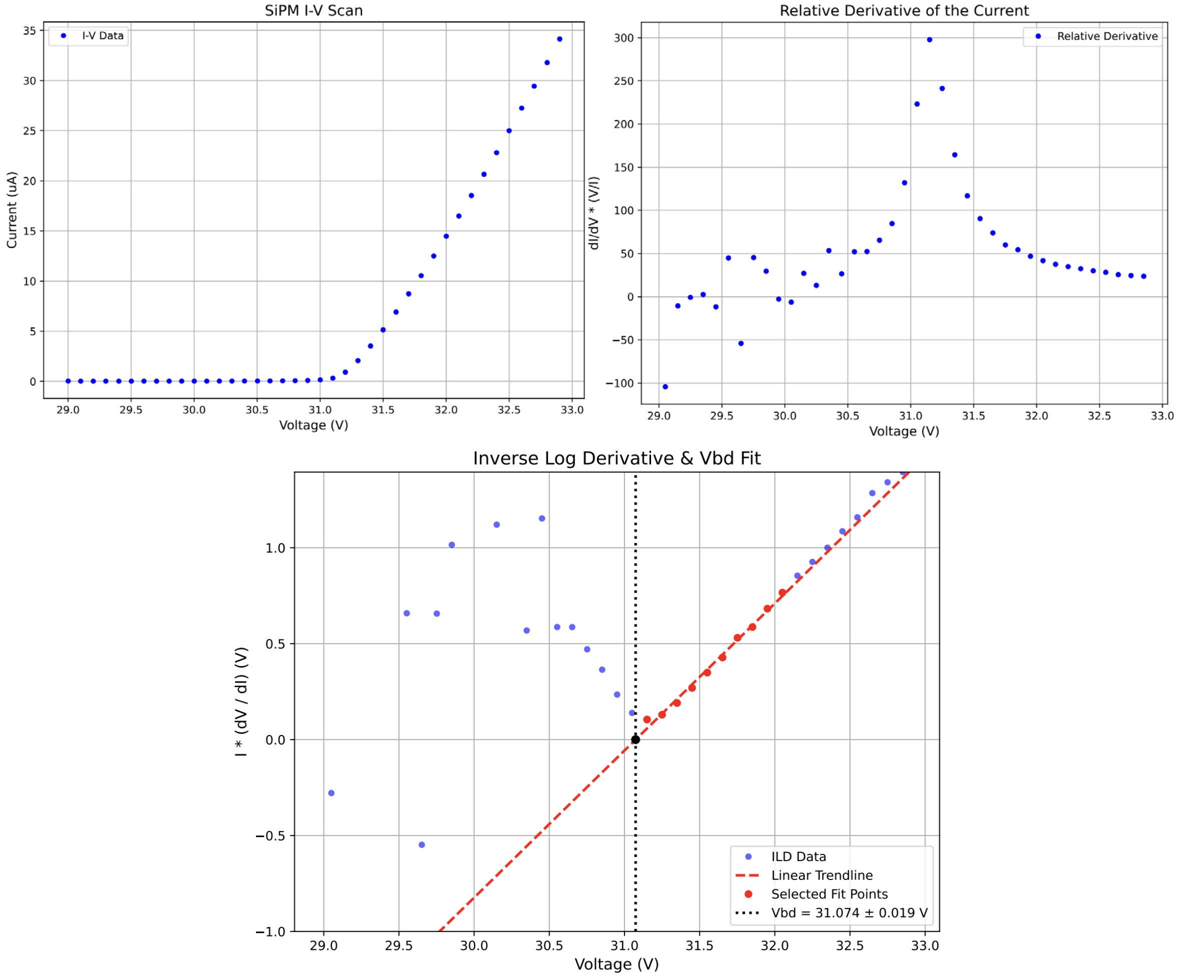

I-V scan (top left), relative derivative (top right), and the Inverse Logarithmic Derivative (bottom)

- Inverse Logarithmic Derivative of the I-V curve

$$\mathrm{ILD}(I(V)) = \left(\frac{d}{dV}\ln I\right)^{-1} = I\frac{dV}{dI}$$

- Scales linearly with the OV above V_{bd}

$$\mathrm{ILD}(I(V)) = \frac{1}{1+\kappa}(V - V_{\mathrm{bd}})$$

- Obtainable by firstly calculate the relative derivative of *I(V)*: $\frac{dI}{dV} \times \frac{V}{I}$

- Then take the inverse and multiply by voltage; the linear fit gives V_{bd}

- Non-irradiated sensors: measured under illumination (dark current too small)

Camera Noise Subtraction

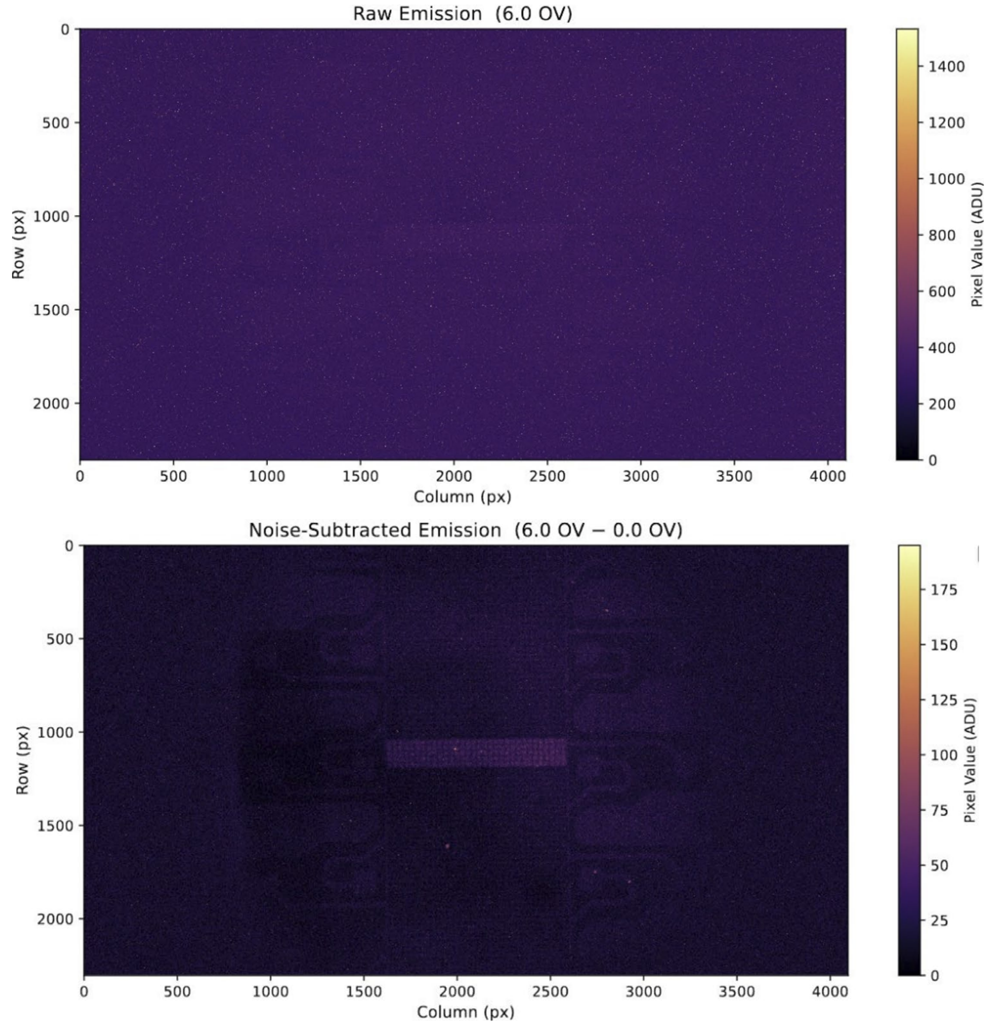

Raw image (top), and noise subutracted image (bottom) for non-irradiated Hamamatsu SiPM at 6.0 OV

- qCMOS fixed-pattern noise: persistently bright defect pixels
- Unbiased dark frame (same 10-min exposure) subtracted from every emission image
- Comparing the two plots, the background colored in purple largely removed
- Cleaner result validates the fixed-additive-offset assumption

Grid Identification & Channel Merging

- Rotation correction to align the cell boarders with the pixel orientation
- Row / column pixel brightness analysed to identify cell borders
- Boarder misalignment ~2 px ≪ wall ~10 px negligible for the purpose of this study
- With 20x objective lens, two half-channel images merged to form the complete EMMI for the channel

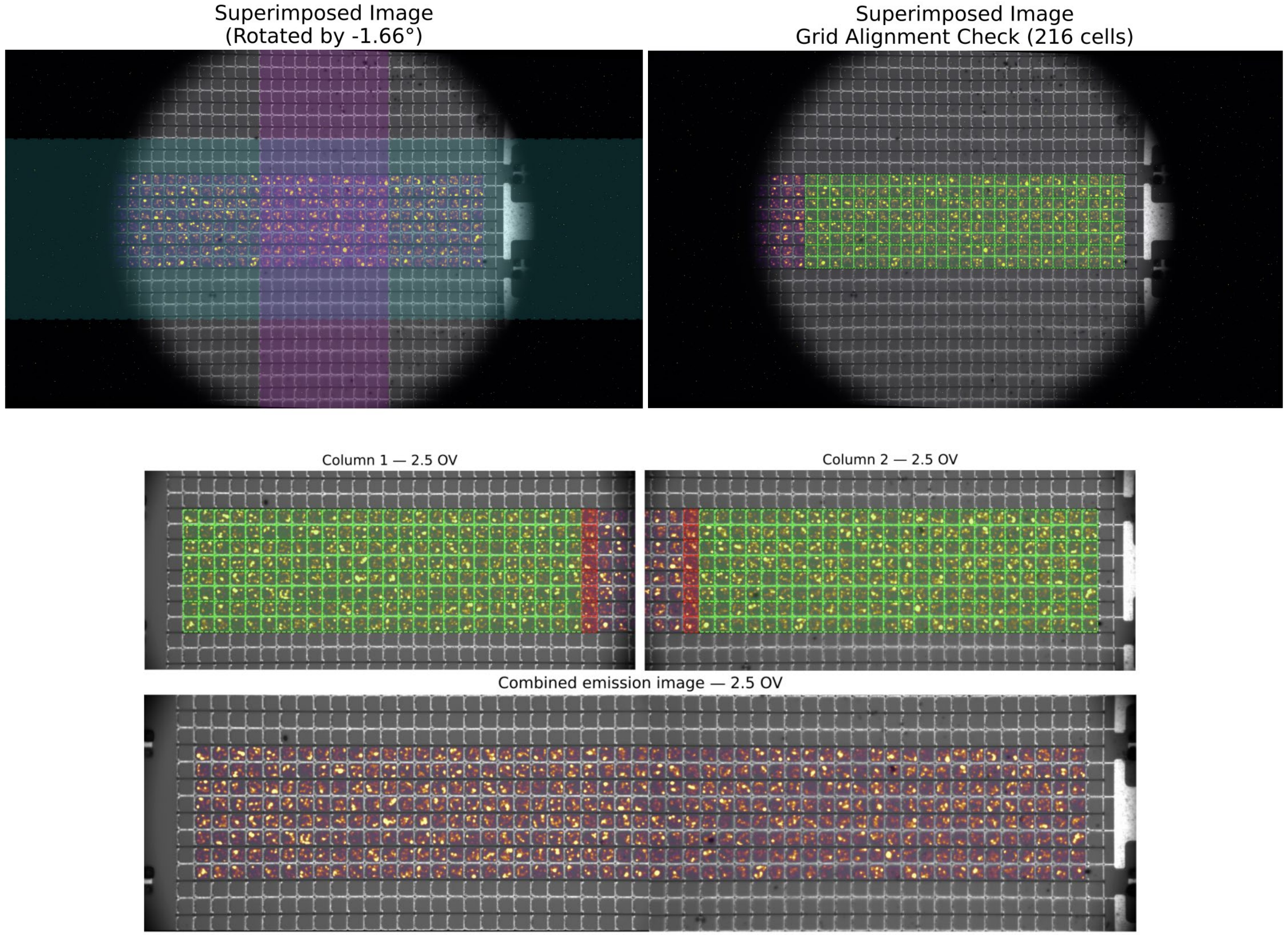

Grid detection (top); merging the two channel halves (bottom)

Hotspot Extraction

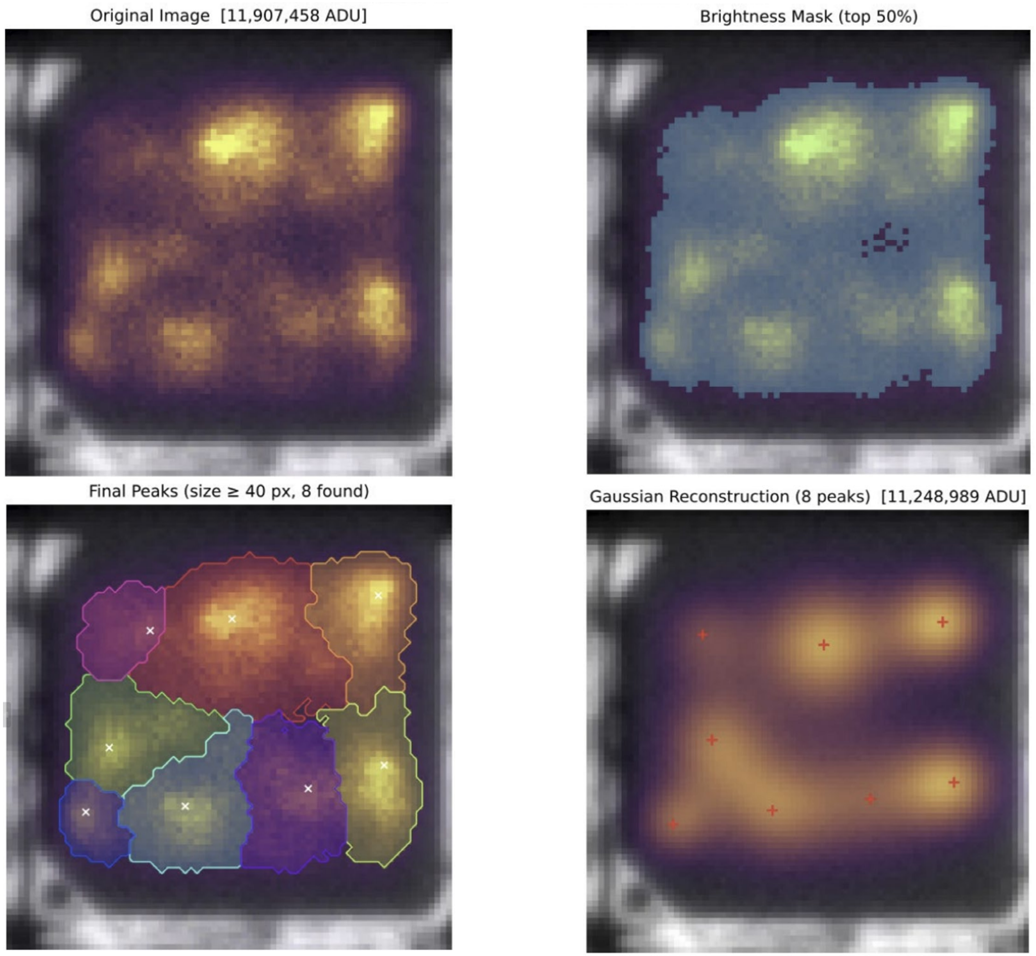

Four-step reconstruction: active pixel threshold, peak finding, watershed segmentation, and 2D Gaussian conversion

- Adaptive percentile threshold to allow active-pixel mask (robust for dim hotspots)
- **peak_local_max** → **watershed**: pixels assigned per peak
- Each peak are reconstructed using 2D Gaussian:
  - **location** = intensity-weighted mean
  - **amplitude** = mean of 3 brightest pixels
  - **σ** = area-matched integrated intensity
- Global rescale of reconstruction → ~5% amplitude bias (known limitation)

Reconstruction Validation

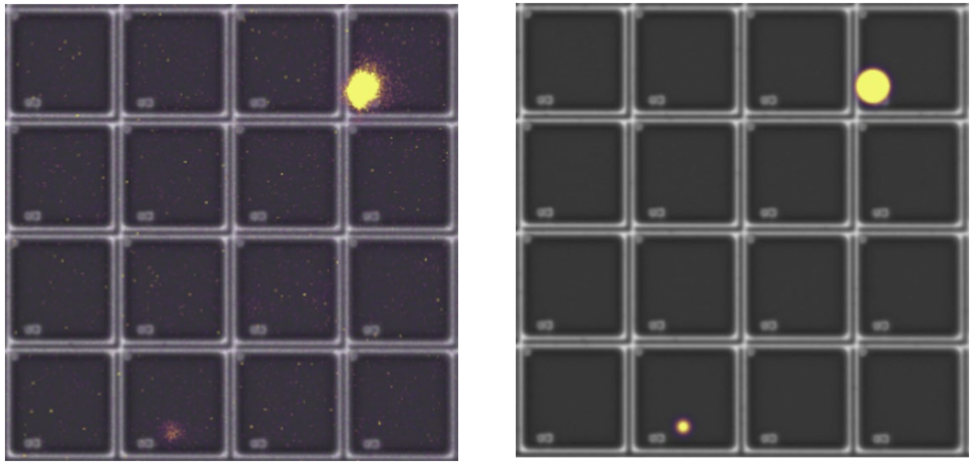

Low density — non-irradiated Hamamatsu @ 10.0 OV
Left: Original EMMI; Right: Gaussian reconstruction

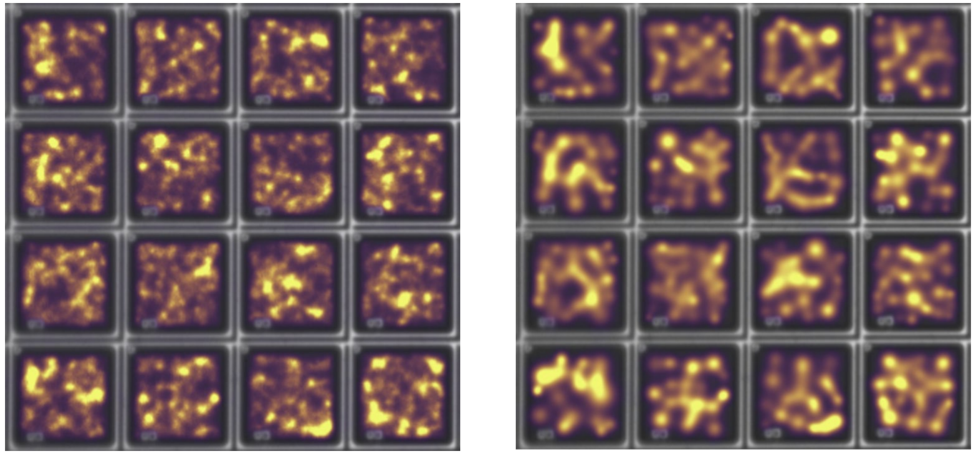

High density — Hamamatsu 1×10^{13} neq/cm² @ 2.5 OV
Left: Original EMMI; Right: Gaussian reconstruction

- Validated in two extreme regimes:
  - **Sparse** (non-irradiated, 10 OV)
  - **Crowded** (1×10^{13}, 2.5 OV)
- Both low density and high density show emission intensity reproduced faithfully
- In the case of high density, algorithm is limited in identifying closely positioned hotspots
- Potentially **Figure of Merit** could be developed (e.g. pixel-wise squared-intensity difference between original and reconstructed images)

Dark I–V vs Fluence

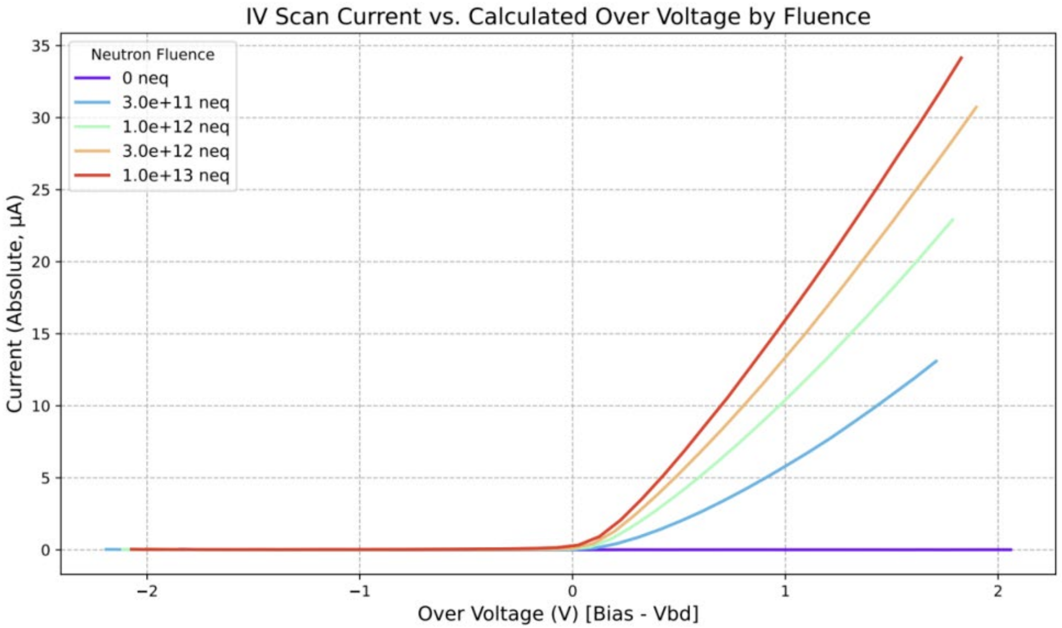

FBK

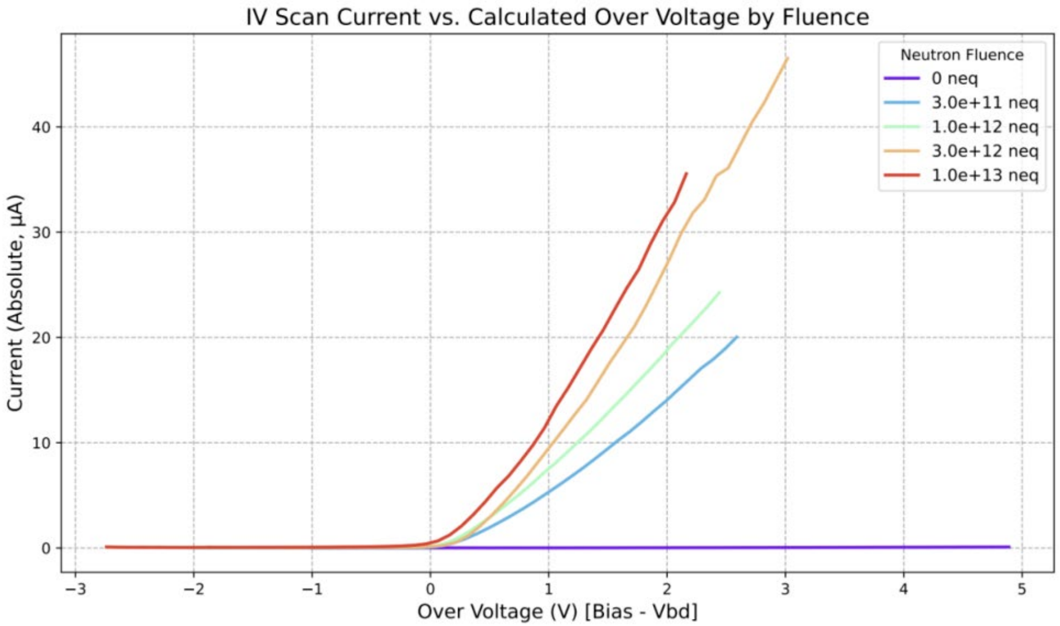

Hamamatsu

- Current at fixed OV rises with fluence, but sub-linearly
- Cause: Recovery-time saturation, cells re-fire before fully recharging
- **Effective OV < nominal at high fluence** — caution for fixed-OV comparisons

Per-Cell Emission Intensity

Non-irradiated FBK @ 10.0 OV

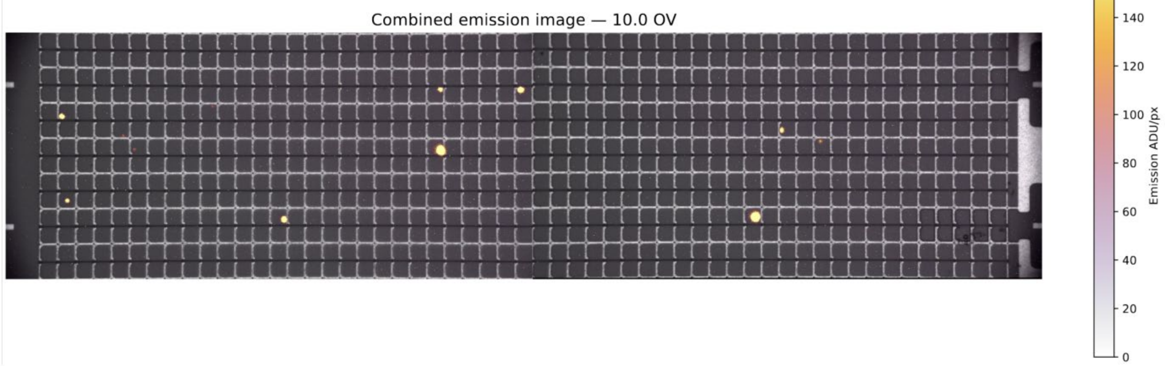

FBK 1×10¹³ neq/cm² @ 2.5 OV

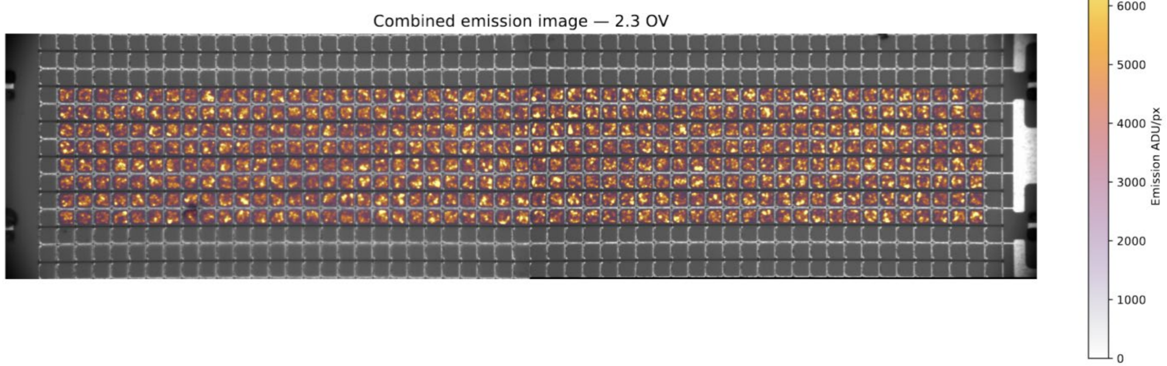

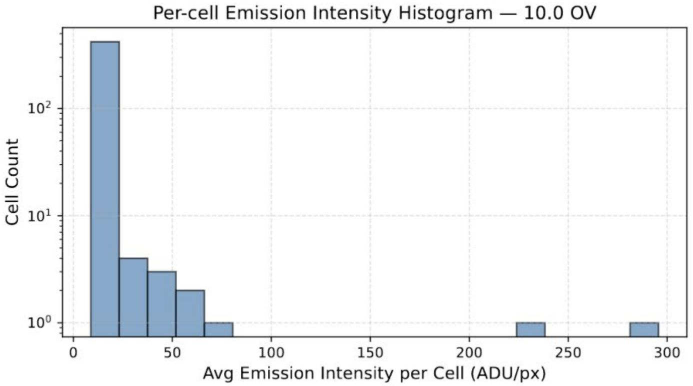

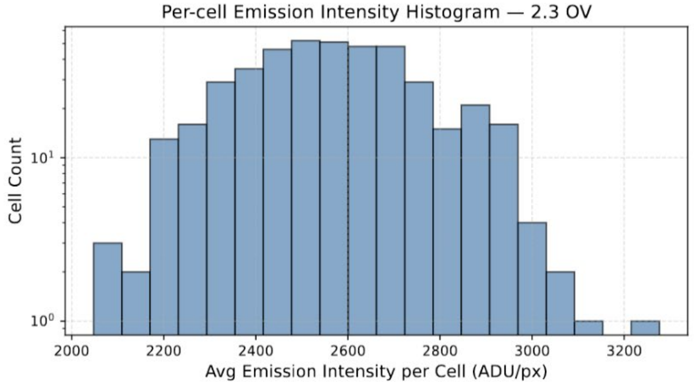

- Non-irradiated FBK: two outlier cells 4–5× brighter than the rest → isolated manufacturing defects
- Irradiated at 1×10^{13}: spatially uniform emission across the channel
- Homogeneous neutron damage washes out the manufacturing outliers

Emission Intensity ∝ Current

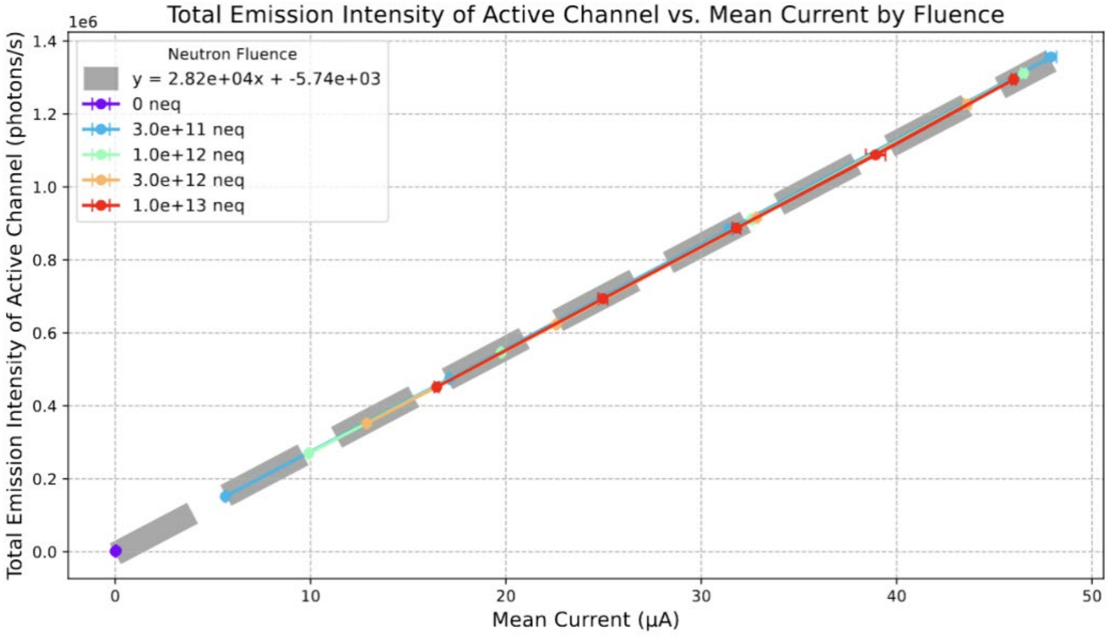

FBK: 2.82×10⁴ photons/μC

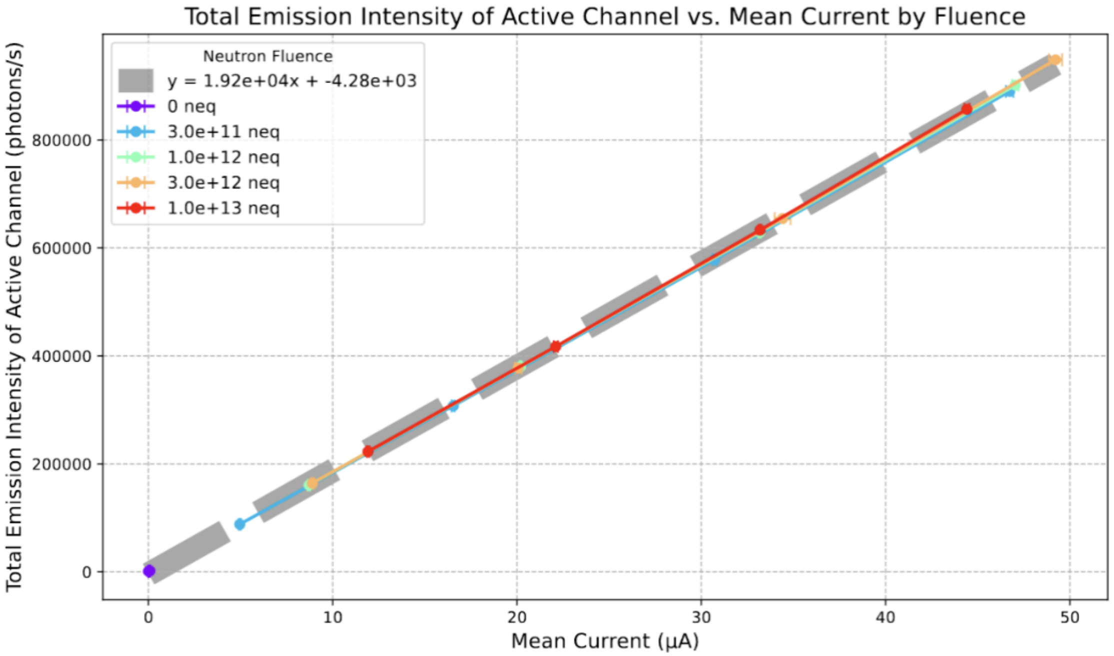

Hamamatsu: 1.92×10⁴ photons/μC

- Total emission vs mean dark current: one single line across all fluences
- Emitted light directly tracks total avalanche charge
- Slopes: 2.82×10^4 (FBK) and 1.92×10^4 (HPK) photons/μC
- Detected yield: **4.51×10^{-9}** (FBK) and **3.07×10^{-9}** (HPK) photons detected per charge carrier

Photons Produced per Charge Carrier

- Obtaining produced photon number requires correcting for the full optical chain
- **Ingredients**: camera QE × emission spectrum × emission-angle acceptance × attenuation × interface reflections

$A(\lambda)$: photon acceptance correction factor

- QE from the manufacturer
- Emission spectrum adopted from a previous study

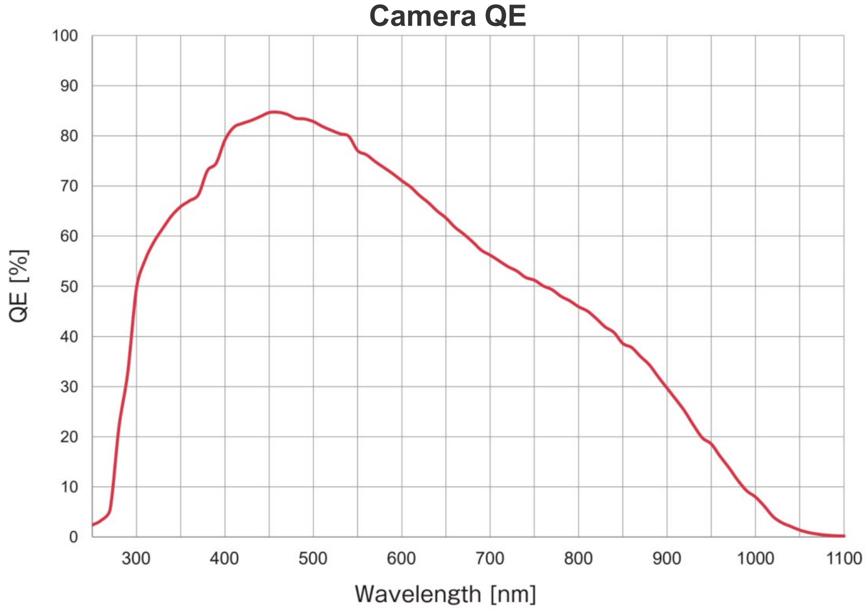

Hamamatsu Photonics K.K. ORCA-Quest 2 qCMOS® camera C15550-22UP Product Brochure. Tech. rep. [Online; accessed 25-June-2026]. 2025.

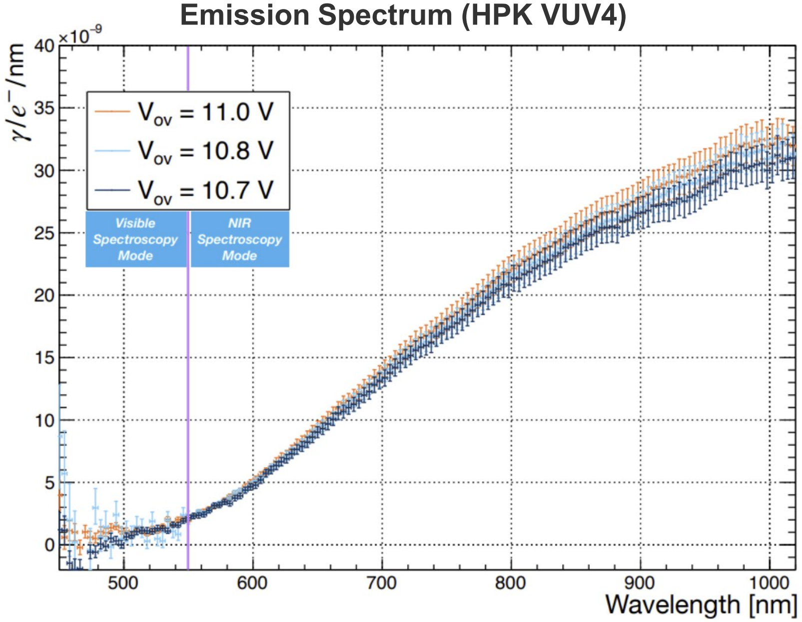

J. B. McLaughlin et al. "Characterisation of SiPM Photon Emission in the Dark". In: Sensors 21.17 (2021), p. 5947. doi: 10.3390/s21175947.

Photons Produced per Charge Carrier

$$A(\lambda) = \frac{\int_0^{2\pi} d\phi}{\int_0^{2\pi} d\phi \int_0^{\pi} \sin\theta \, d\theta} \int_0^{\theta_{\mathrm{Si}}} e^{-\frac{d_{\mathrm{P}}}{\cos\theta\,\mu(\lambda)}} \left(1 - R_{\mathrm{Si,SiO_2}}(\lambda,\theta)\right)\left(1 - R_{\mathrm{SiO_2,Atm}}(\lambda,\theta')\right) \sin\theta \, d\theta$$

$$= \frac{1}{2} \int_0^{\theta_{\mathrm{Si}}} e^{-\frac{d_{\mathrm{P}}}{\cos\theta\,\mu(\lambda)}} \left(1 - R_{\mathrm{Si,SiO_2}}(\lambda,\theta)\right)\left(1 - R_{\mathrm{SiO_2,Atm}}(\lambda,\theta')\right) \sin\theta \, d\theta,$$

Acceptance Angle

Reflectivity

Attenuation

J. B. McLaughlin et al. "Characterisation of SiPM Photon Emission in the Dark". In: Sensors 21.17 (2021), p. 5947. doi: 10.3390/s21175947.

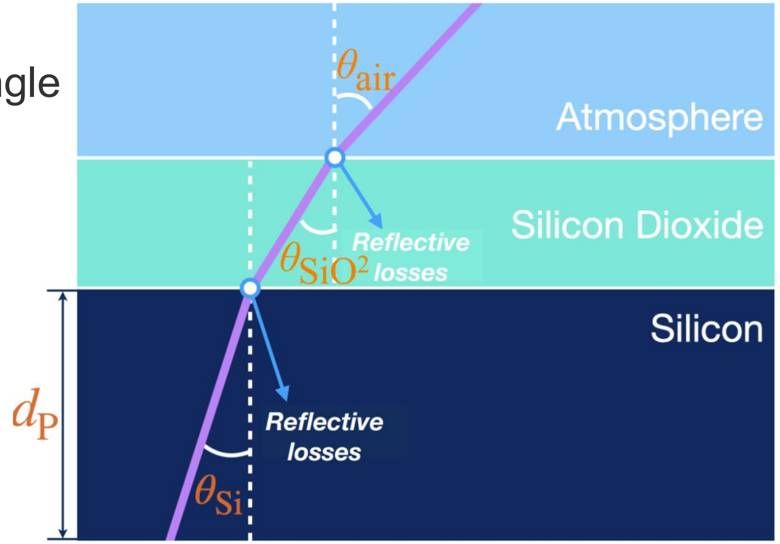

- *A(λ)* integrates slant-path attenuation and reflection losses over the collected solid angle
- Overall detection efficiency: 0.076% (FBK), 0.062% (HPK)
- **5.98×10^{-6} (FBK) and 4.92×10^{-6} (HPK) photons produced per charge carrier**
- Order-of-magnitude agreement with McLaughlin et al. [2021] (~5×10^{-6} / ~8×10^{-6})

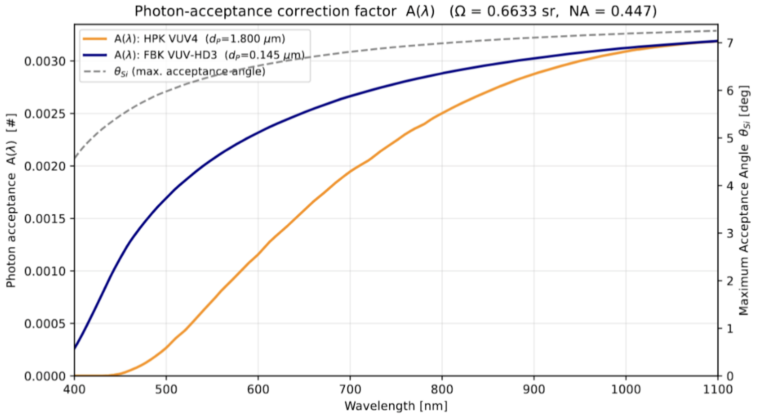

Photon acceptance A(λ)

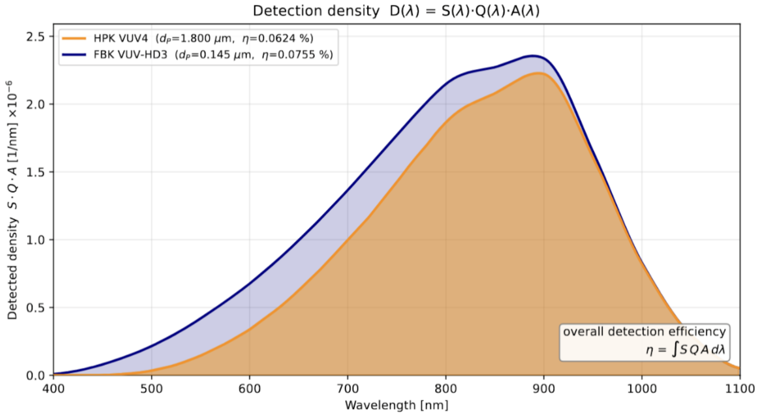

Overall detection density

Hotspot Density (vs OV)

Hotspot density — FBK

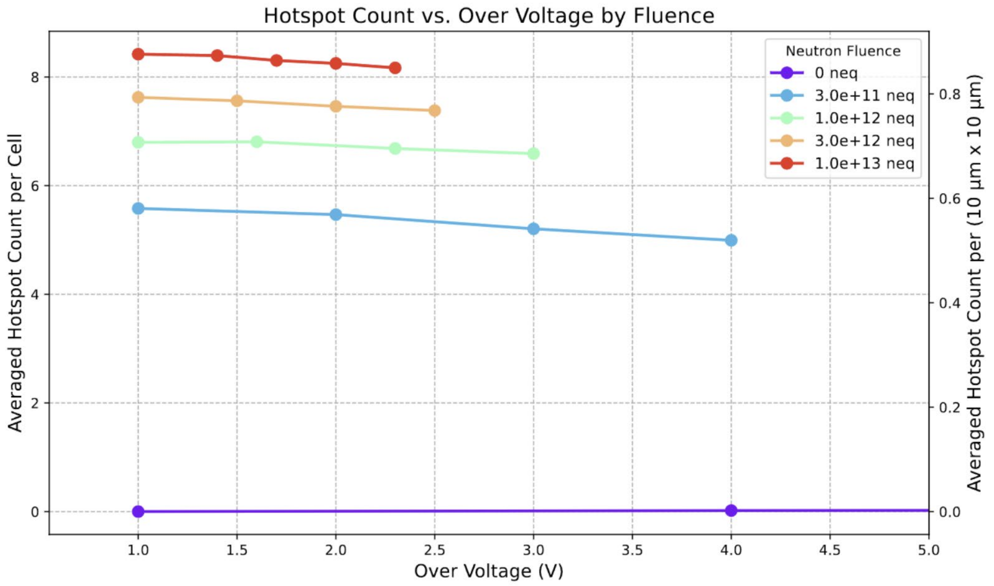

Hotspot density — Hamamatsu

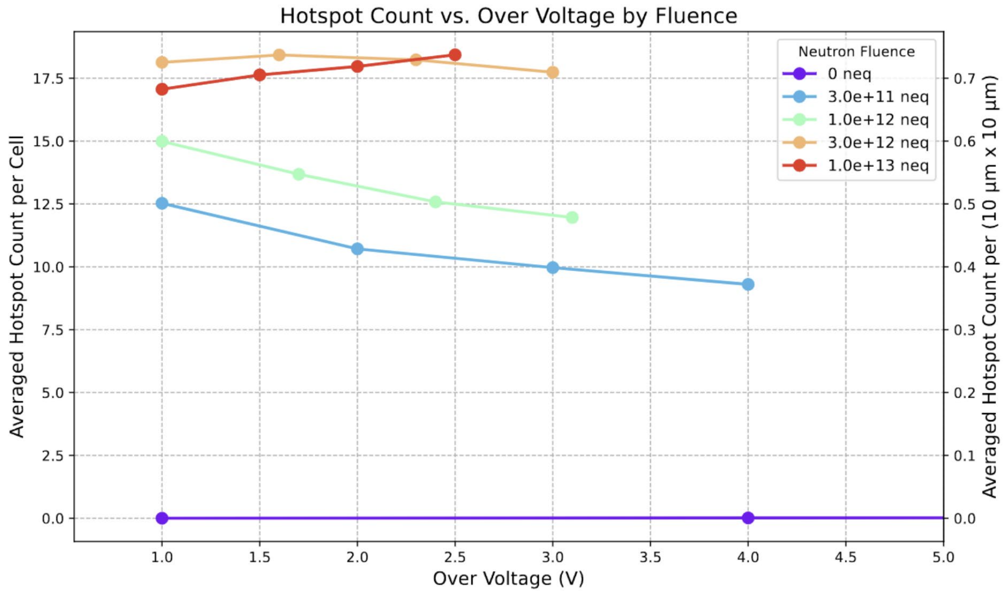

- Clear ordering with fluence for both manufacturers
- In general decreasing trend → hotspot size increases with OV and merge together
- Since Hamamatsu hotspots deeper, dim hotspots are hardly differentiated at high density
- Counts roughly flat vs OV → sites are fixed, not field-induced

Hotspot Density (vs Fluence)

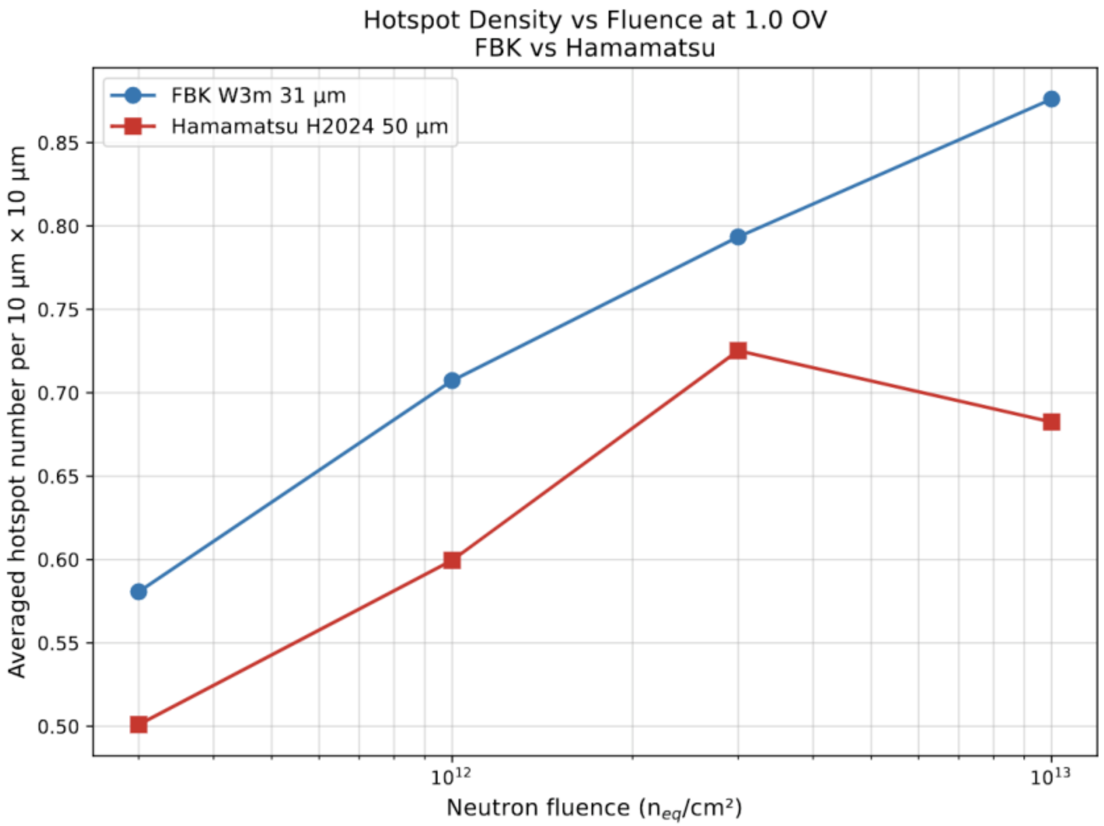

Area-normalised hotspot density @ 1.0 OV

- Hotspot density at 1.0 OV against different fluences
- FBK: 0.58 → 0.88 hotspots per $(10\ \mu m)^2$, monotonic rise with fluence
- HPK turnover at 1×10^{13} (0.73 → 0.68): hotspot merging — algorithmic limit, not fewer damage sites
- Difference could associate with algorithm and emission depth difference

Where Does the Damage Sit?

Non-irradiated sensors at 10 OV: FBK 31um (top) and HPK 50um (bottom)

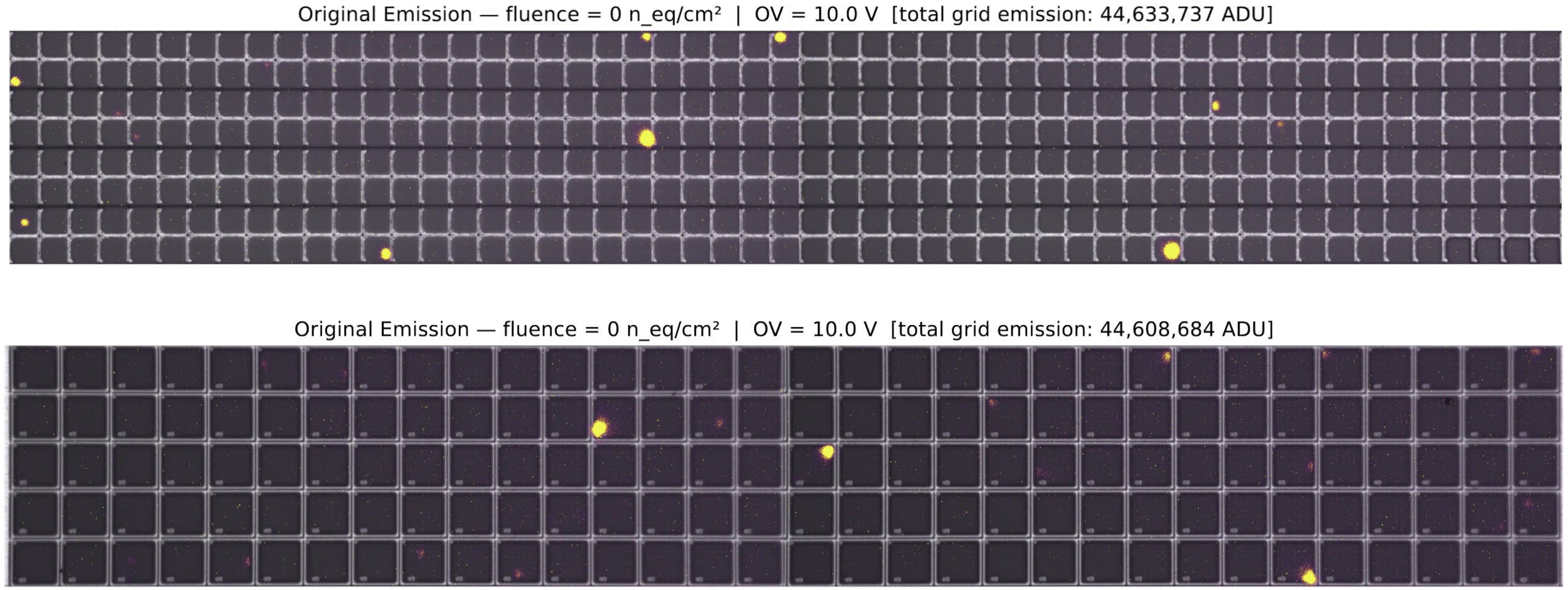

- Only a handful of bright, isolated hotspots per channel
- Hotspots sit predominantly at or near cell borders
- Manufacturing process causes the defects to gather at borders
- Sparse locations at limited cells

Where Does the Damage Sit?

1e13 n_{eq}/cm^2 sensors at highest OV: FBK 31um (top) and HPK 50um (bottom)

Original Emission — fluence = 1e13 n_eq/cm² | OV = 2.3 V [total grid emission: 6,321,344,364 ADU]

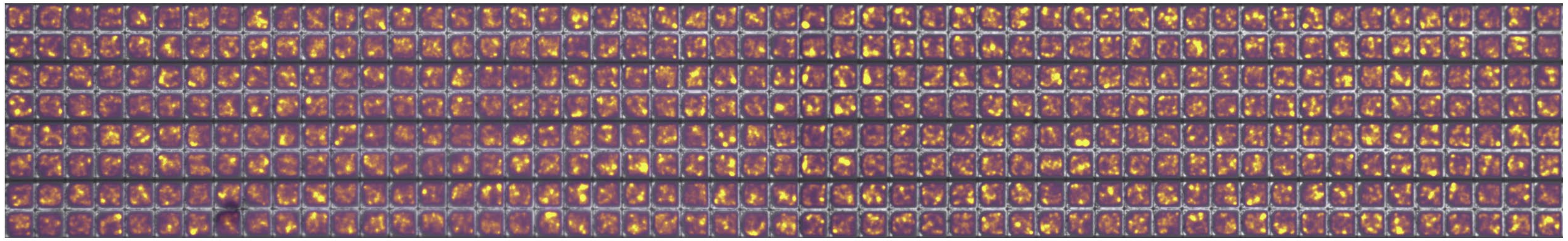

Original Emission — fluence = 1e13 n_eq/cm² | OV = 2.5 V [total grid emission: 4,262,096,827 ADU]

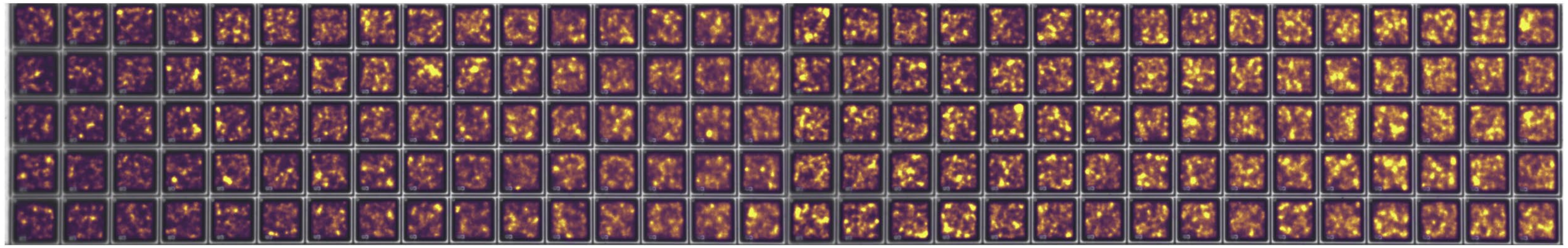

- Evenly spread hotspots across all cells
- Large quantity needs statistical analysis
- Information from extracted 2D Gaussians are used

Where Does the Damage Sit?

In-cell hotspot positions @ 1×10¹³: FBK (left), HPK (right)

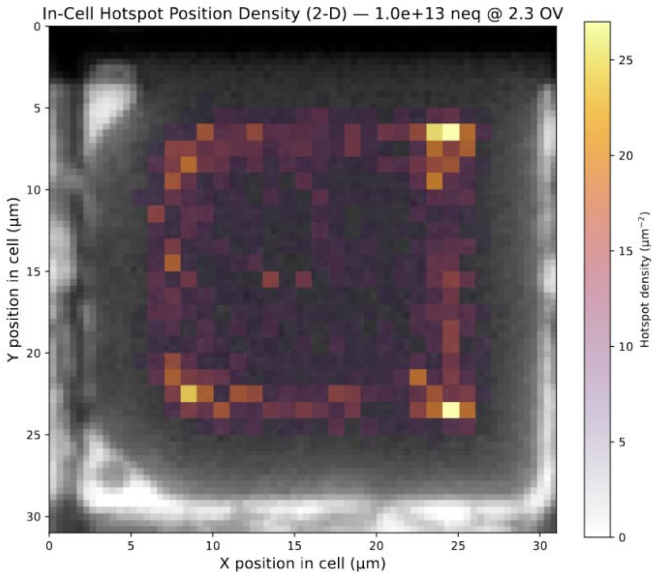

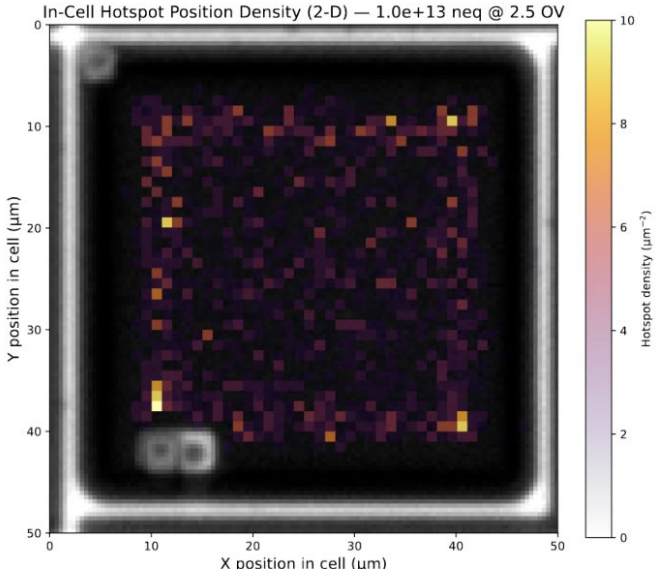

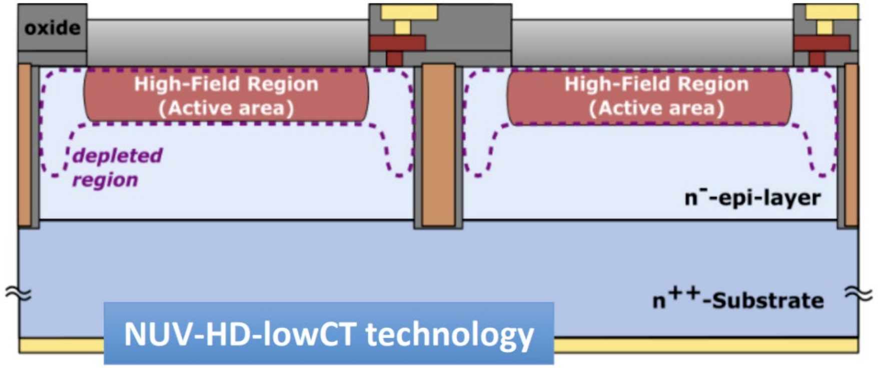

- Intensity-weighted centres

$$\bar{x} = \frac{\sum_i x_i I_i}{\sum_i I_i}, \quad \bar{y} = \frac{\sum_i y_i I_i}{\sum_i I_i}$$

- Hotspots cluster in a square ring inside each cell close to the boarders
- Interpretation: carriers from the depletion region drift into the multiplication volume
- Corner structure especially vulnerable. Round-shaped cells could potentially mitigate this

F. Acerbi. SiPM rad-hard R&D: AIDAinnova production at FBK. Presentation at Fondazione Bruno Kessler (FBK). Presented on 2025-05-14. May 2025.

Fill Factor Estimation

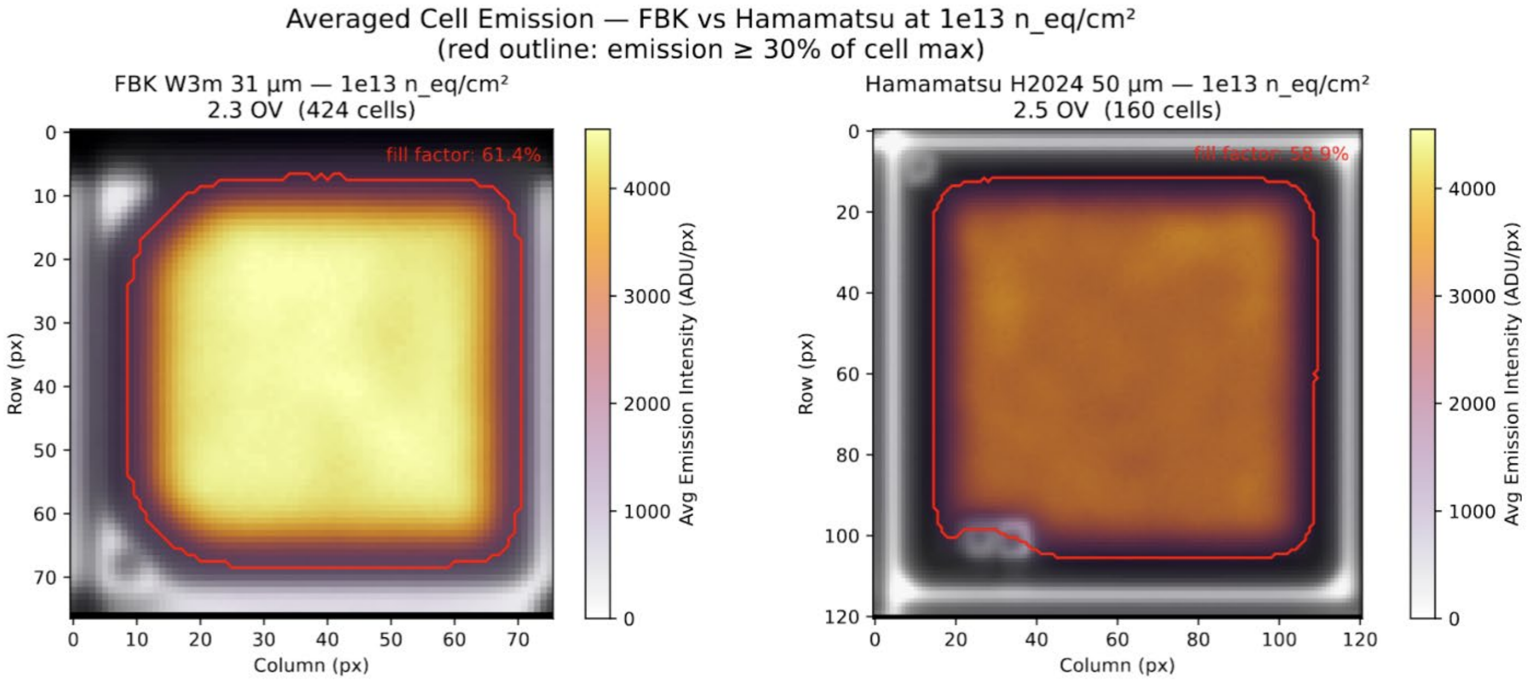

Averaged cell emission @ 1×10¹³, highest OV — FBK (left), Hamamatsu (right)

- Averaged cell emission at 1×10^{13} used as a functional map of the active area
- Active area defined as the contiguous region emitting > 30% of peak intensity
- FBK 31 µm → **61.4%** (77.7% claimed); Hamamatsu 50 µm → **58.9%** (68.2% previously measured)
- These are lower bounds: depletion-region drift enlarges the effective photosensitive area

Conclusions & Outlook

- **Achieved**
  - Reproducible EMMI pipeline: ILD V_{bd}, auto grid alignment, watershed → 2D-Gaussian hotspots
  - Able to extract hotspot density, intensity, size information, etc.
  - Emission ∝ current; 5.98 / 4.92 $\times 10^{-6}$ (FBK / HPK) photons per carrier — literature-consistent
  - Hotspot position pattern and potential cause analysed
  - Fill factor lower bounds: 61.4% / 58.9% (FBK / HPK)

- **Outlook**
  - Reconstruction figure of merit + fitting parameter fine tuning → remove ~5% bias
  - Investigate in systematic correlation between each extracted metric and radiation damage
  - Compare same-size cells, as well as investigate in round-shaped cells
  - **EMMI as a cell-level diagnostic for LHCb Upgrade II & future experiments**

Thank you!

Lai Gui — LPHE, EPFL

Backup Slides

SRH Generation & DCR

- Perfect crystal: generation needs full Eg ≈ 1.12 eV → strongly suppressed
- Defects (manufacturing or displacement damage) → localised mid-gap states
- Shockley–Read–Hall: valence → trap → conduction in two smaller steps → generation rate greatly enhanced
- DCR contributions:
    - Temperature: DCR ∝ $\exp(-E_a / kT)$
    - Overvoltage: higher field → higher trigger probability
    - Fill factor: larger active volume → more thermal generation
    - Radiation: traps also act as trap-assisted-tunnelling (TAT) centres

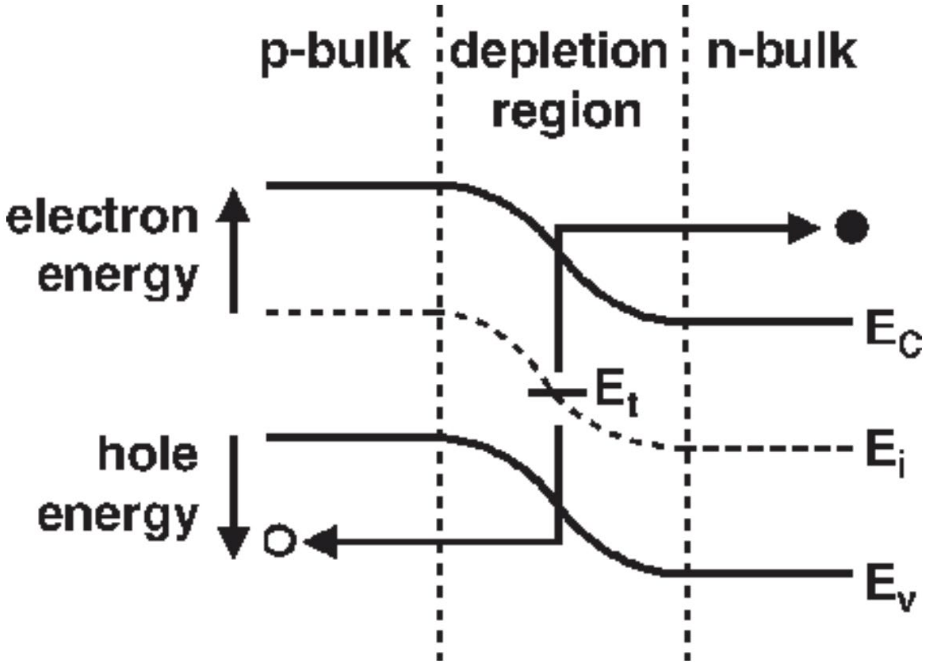

SRH middle gap states create SRH carriers in the depleted volume that can trigger avalanche

Photon Acceptance Factor A(λ)

$$A(\lambda) = \frac{\int_0^{2\pi} d\phi}{\int_0^{2\pi} d\phi \int_0^{\pi} \sin\theta \, d\theta} \int_0^{\theta_{\mathrm{Si}}} e^{-\frac{d_{\mathrm{P}}}{\cos\theta\,\mu(\lambda)}} \left(1 - R_{\mathrm{Si,SiO_2}}(\lambda,\theta)\right)\left(1 - R_{\mathrm{SiO_2,Atm}}(\lambda,\theta')\right) \sin\theta \, d\theta$$

$$= \frac{1}{2} \int_0^{\theta_{\mathrm{Si}}} e^{-\frac{d_{\mathrm{P}}}{\cos\theta\,\mu(\lambda)}} \left(1 - R_{\mathrm{Si,SiO_2}}(\lambda,\theta)\right)\left(1 - R_{\mathrm{SiO_2,Atm}}(\lambda,\theta')\right) \sin\theta \, d\theta,$$

$$\mathrm{NA} \equiv n_{\mathrm{air}} \sin\theta_{\mathrm{air}} = n_{\mathrm{SiO_2}} \sin\theta_{\mathrm{SiO_2}} = n_{\mathrm{Si}} \sin\theta_{\mathrm{Si}},$$

$$\therefore \quad \theta_{\mathrm{Si}} = \sin^{-1}\left(\frac{\mathrm{NA}}{n_{\mathrm{Si}}}\right),$$

- Attenuation along slant path from production depth d_P; $\mu(\lambda)$ = absorption length in Si
- Fresnel losses at Si/SiO_2 and SiO_2/air interfaces; θ′ from Snell's law
- d_P from Gallina et al. [2019]: 1.8 ± 0.1 μm (HPK H2017), 0.145 ± 0.01 μm (FBK LF)
- SiO_2 absorption neglected (long absorption length)

(θ_{air} = 26.57°, 20× objective)

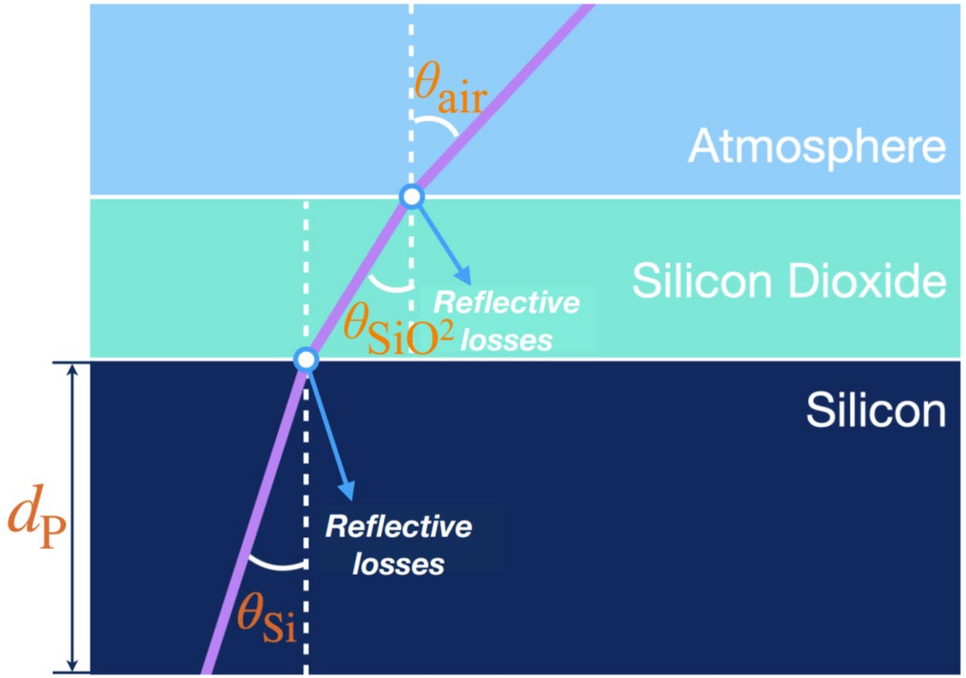

Refraction/reflection geometry through the Si / SiO_2 / air stack

Reflectivities & Optical Constants

$$R = \frac{1}{2}\left(|r_s|^2 + |r_p|^2\right) \qquad r_s = \frac{n_1 \cos\theta_1 - n_2 \cos\theta_2}{n_1 \cos\theta_1 + n_2 \cos\theta_2}, \qquad r_p = \frac{n_2 \cos\theta_1 - n_1 \cos\theta_2}{n_2 \cos\theta_1 + n_1 \cos\theta_2}$$

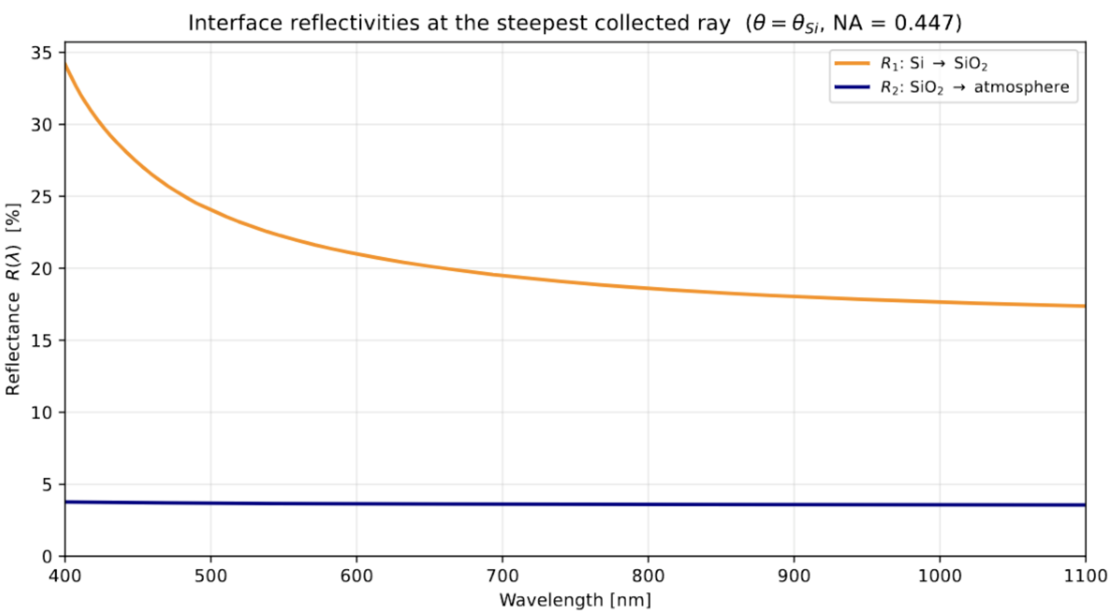

Fresnel reflectivity at max collectable angle (unpolarised: R = (|rs|² + |rp|²)/2)

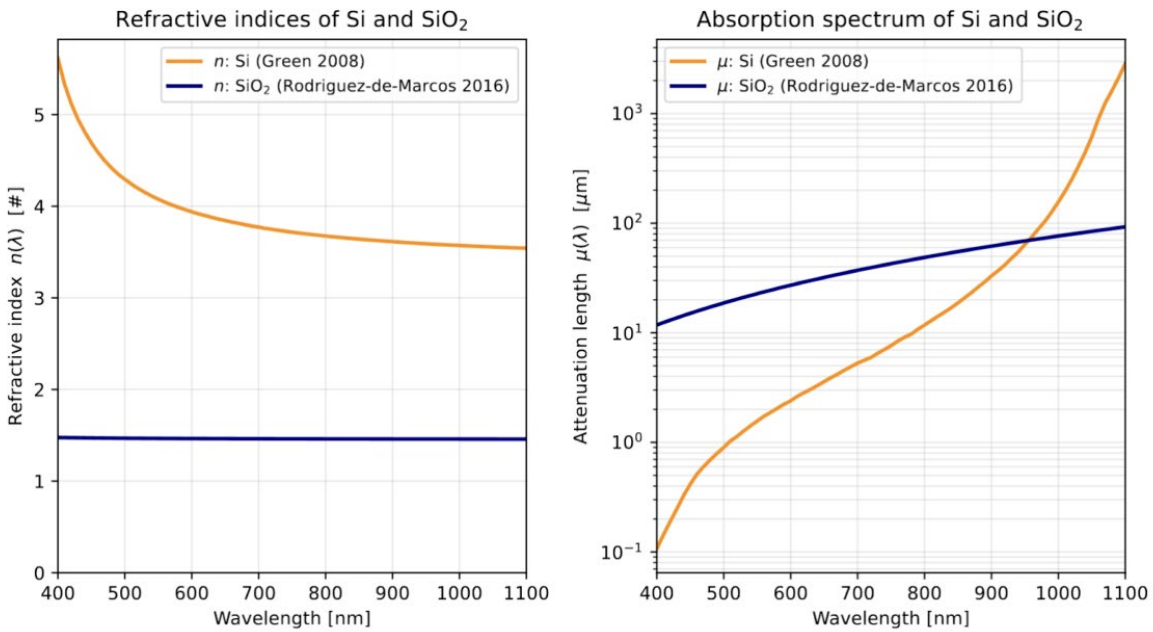

Refractive indices & absorption lengths of Si and SiO_2

- Short absorption length in Si (visible/UV) → only near-IR emission escapes from depth dP

Camera QE & Emission Spectrum

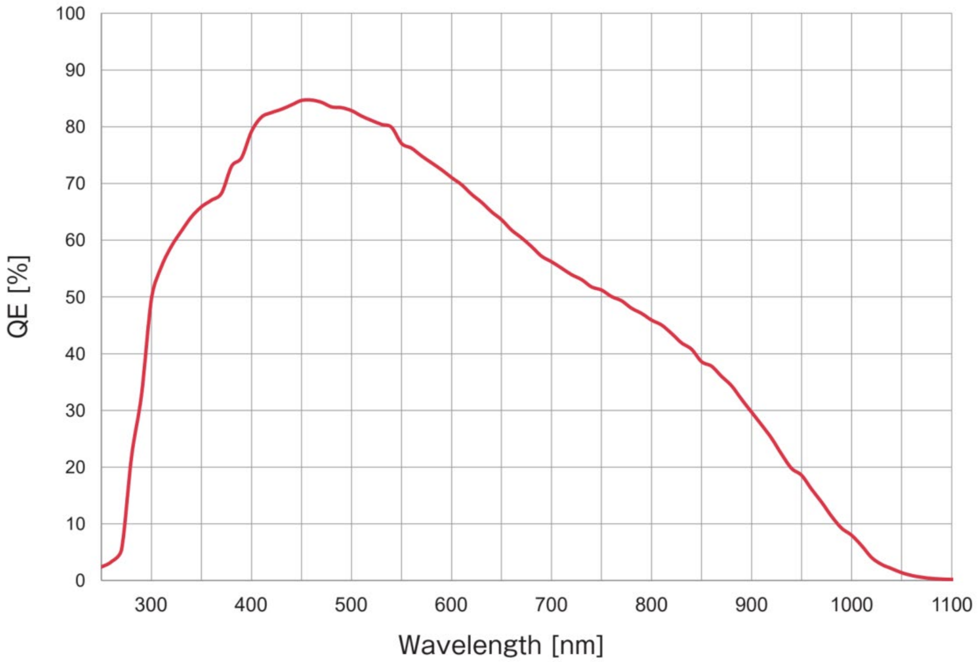

ORCA-Quest 2 QE (manufacturer) — used as PDE

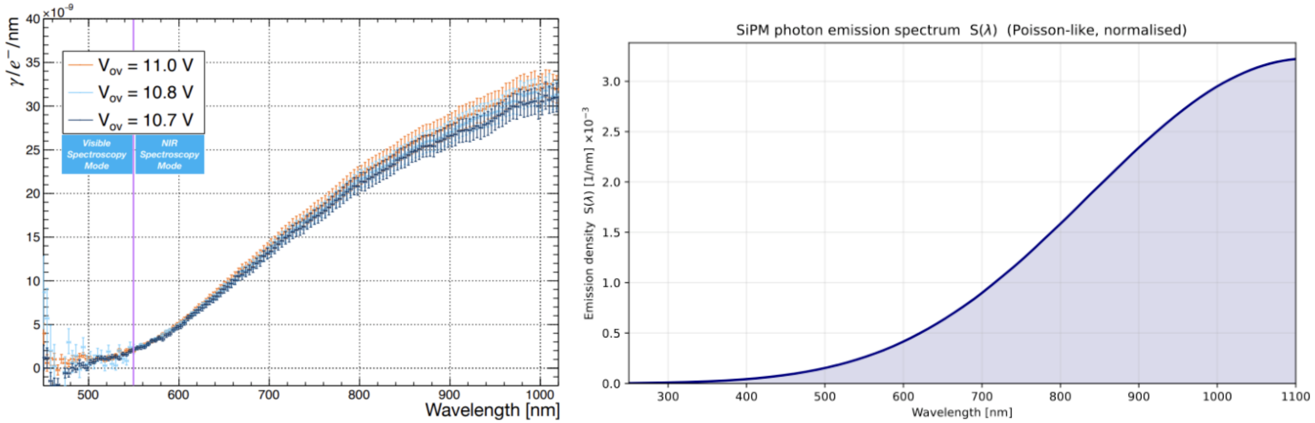

SiPM emission spectrum adopted from McLaughlin et al. (no spectrometer available)

- QE falls steeply in the near-IR → dominates the overall detection efficiency
- Photon-number-resolving mode not used: 200 photons/px limit saturates over 10-min exposures on irradiated samples → HDR readout preferred

Exponentially Modified Gaussian

$$f(x;\mu,\sigma,\lambda) = \frac{\lambda}{2}\exp\left[\frac{\lambda}{2}\left(2\mu + \lambda\sigma^2 - 2x\right)\right]\operatorname{erfc}\left(\frac{\mu + \lambda\sigma^2 - x}{\sqrt{2}\sigma}\right)$$

$$\operatorname{erfc}(x) = 1 - \operatorname{erf}(x) = \frac{2}{\sqrt{\pi}}\int_x^\infty e^{-t^2}\,dt$$

- μ: peak position · σ: Gaussian width · λ: exponential decay rate (positive-tail length)
- Gaussian bulk of typical hotspots + long tail from the brightest damage sites
- Fits intensity, size and current-contribution distributions across all OV & fluences
- MPV of the fit used as the single damage metric per distribution

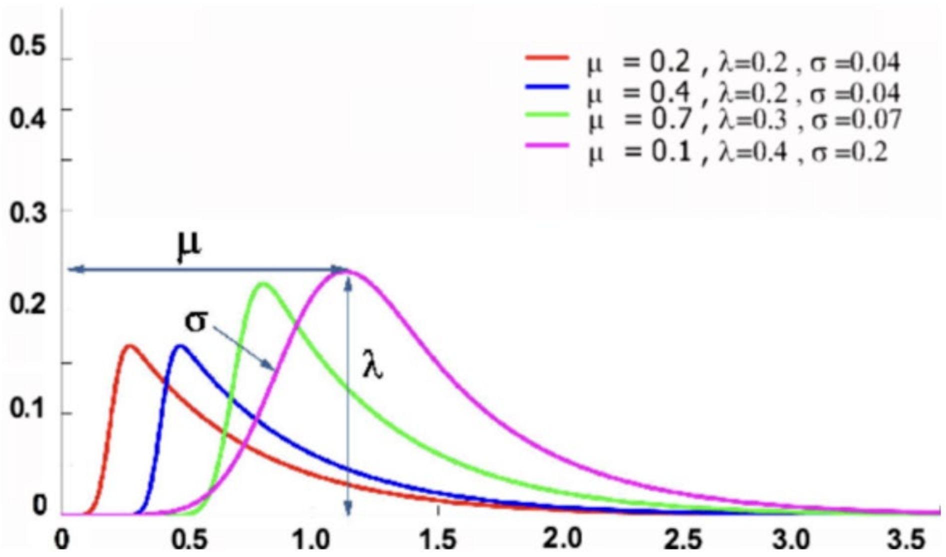

Hotspot Intensity

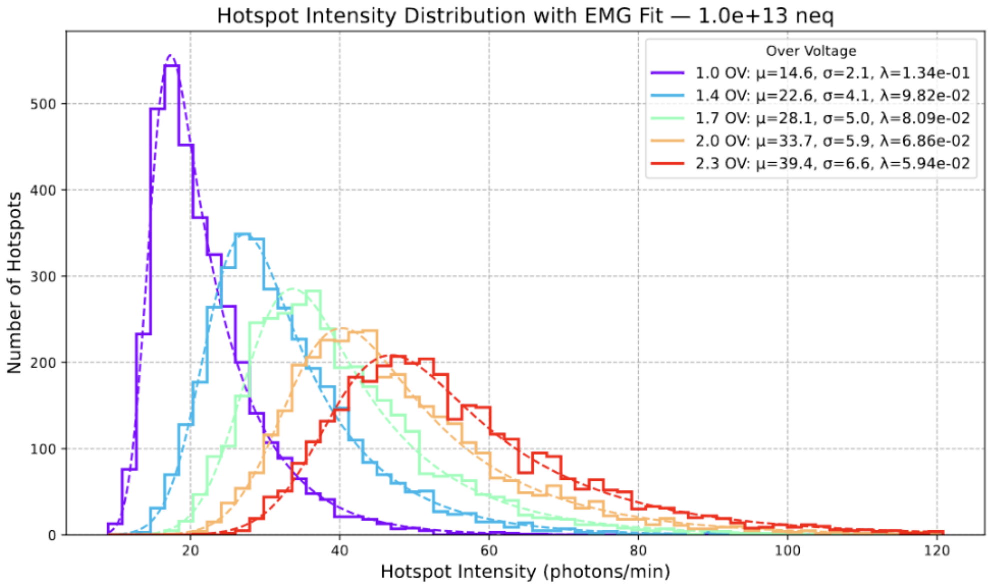

EMG fits — FBK 1×10¹³ neq/cm²

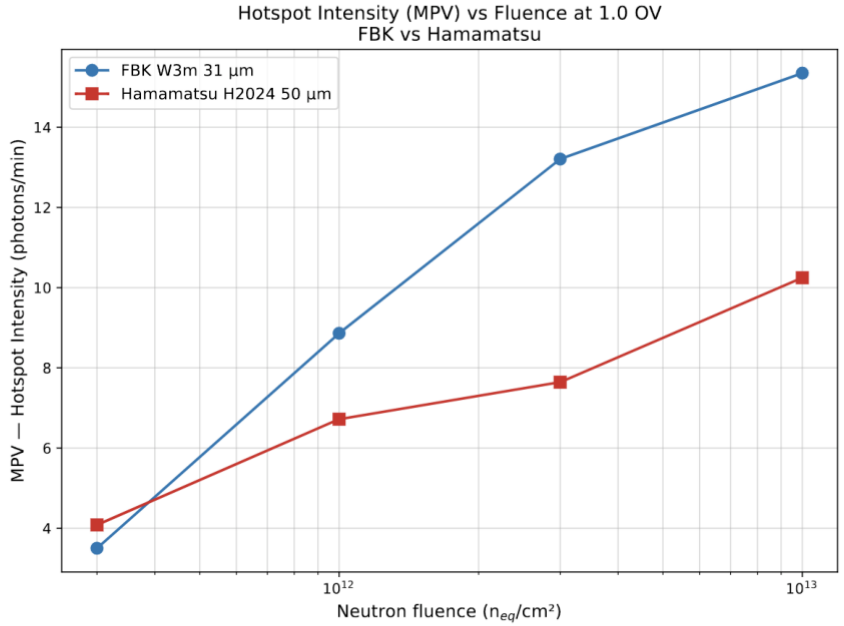

Intensity MPV vs fluence @ 1.0 OV

- Intensity distributions well fit by an Exponentially Modified Gaussian at all OV and fluences
- Gaussian bulk of typical hotspots + exponential tail from the brightest damage sites
- MPV grows with both OV and fluence → candidate non-destructive fluence metric
- FBK rises steeper: ~15 vs ~10 photons/min at 1×10^{13} neq/cm²

Hotspot Size & Current Contribution

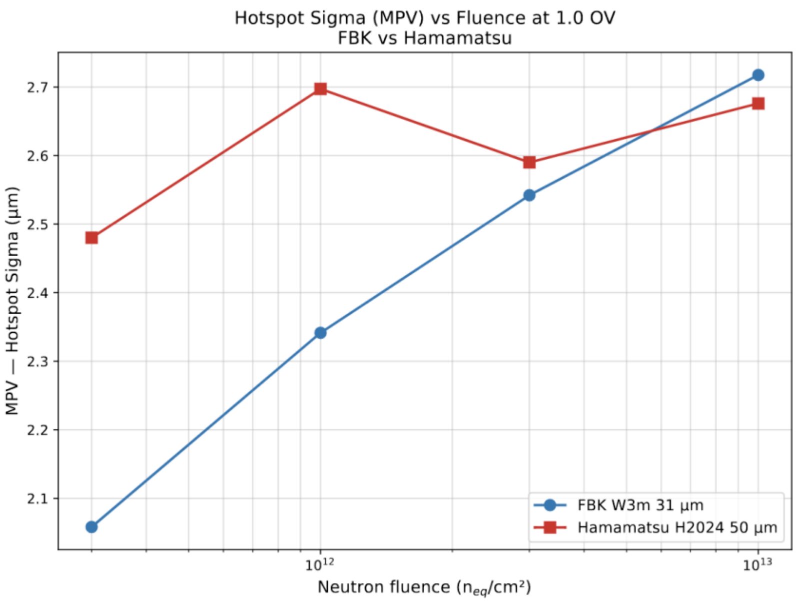

Size (σ) MPV @ 1.0 OV

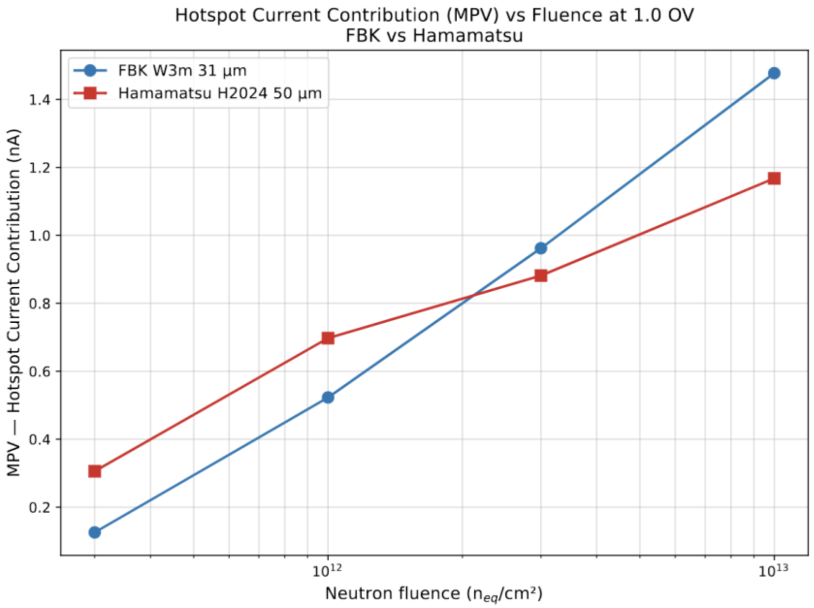

Per-hotspot current MPV @ 1.0 OV

- Size ordering is opposite to intensity: HPK larger at low fluence (~2.5 vs 2.1 μm); both converge to ~2.7 μm
- FBK hotspots grow brighter and broader; HPK mainly brighter
- Per-hotspot current: ~0.1–0.3 nA → ~1.2–1.5 nA across the fluence range
- The two technologies cross near 3×10^{12} neq/cm². FBK grows more rapidly, signifying its vulnerability

In-Cell Position Projections

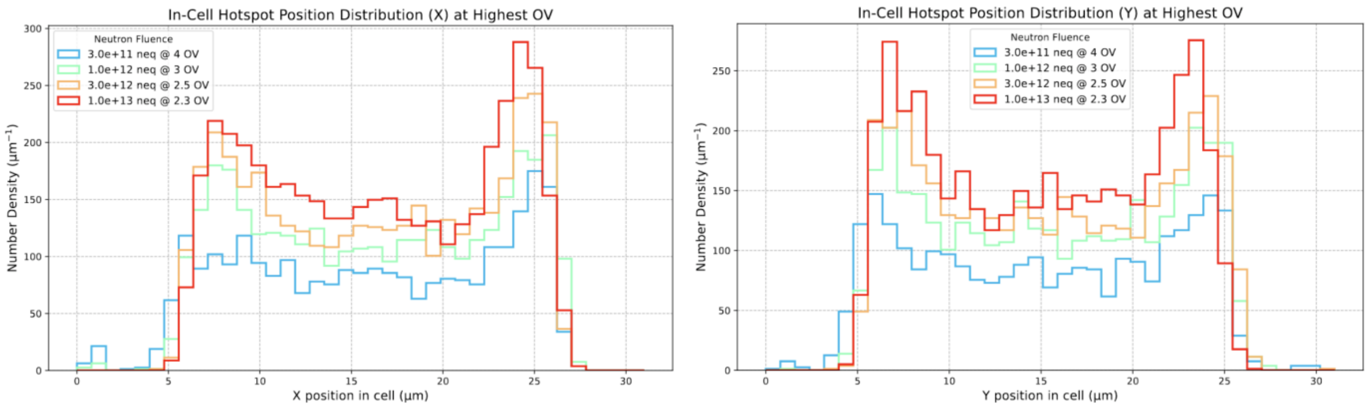

FBK — x / y projections, highest OV

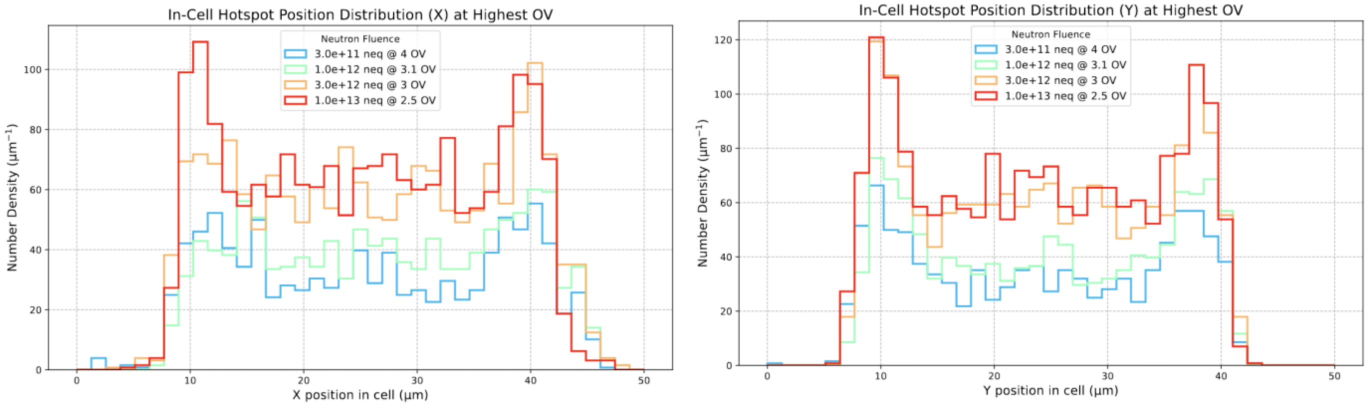

Hamamatsu — x / y projections, highest OV

- Intensity weighted centres:

$$\bar{x} = \frac{\sum_i x_i I_i}{\sum_i I_i}, \quad \bar{y} = \frac{\sum_i y_i I_i}{\sum_i I_i}$$

- Double-peaked in both axes — hotspots avoid the cell centre and the extreme edges
- 1D signature of the square-ring clustering seen in the 2D histograms

Ring Amplitude Uniformity

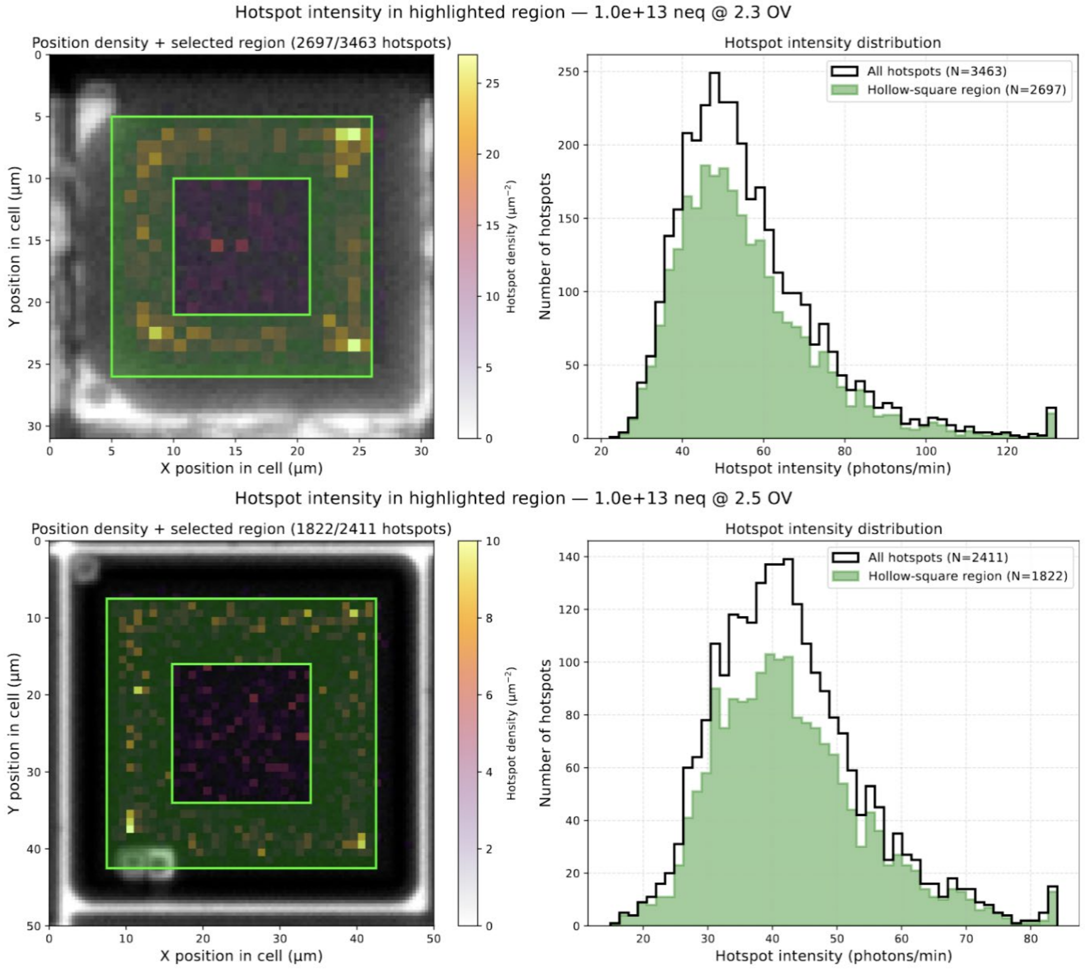

- Hollow-square region selected on the 2D position distribution (FBK top, HPK bottom)
- Amplitude of hotspots inside the ring shows no marked positional bias
- **The ring marks where avalanches are triggered, not where emission is strongest**
- Alternative hypothesis: reconstruction algorithm groups border hotspots into the ring — disentangling left for future work

Pipeline Parameters & Limitations

- **Hand-tuned parameters**
  - **DETECTION_THRESHOLD_PCT** — percentile for the active-pixel mask
  - **MIN_DISTANCE** — minimum separation between local maxima (drives the count systematics)
  - **N_PEAK_BRIGHTNESS** — pixels used for the amplitude
  - **MIN_PEAK_SIZE** — minimum peak size to reconstruct
- **Known limitations**
  - Overlapping Gaussians → global rescale → ~5% amplitude bias
  - Peak merging at high OV / high fluence → apparent count drops
  - No figure of merit for reconstruction quality yet (candidate: pixel-wise squared-intensity residual)
- **With an Figure of Merit + more computing: parameter optimisation and potentially simultaneous Gaussian fitting → bias-free extraction**

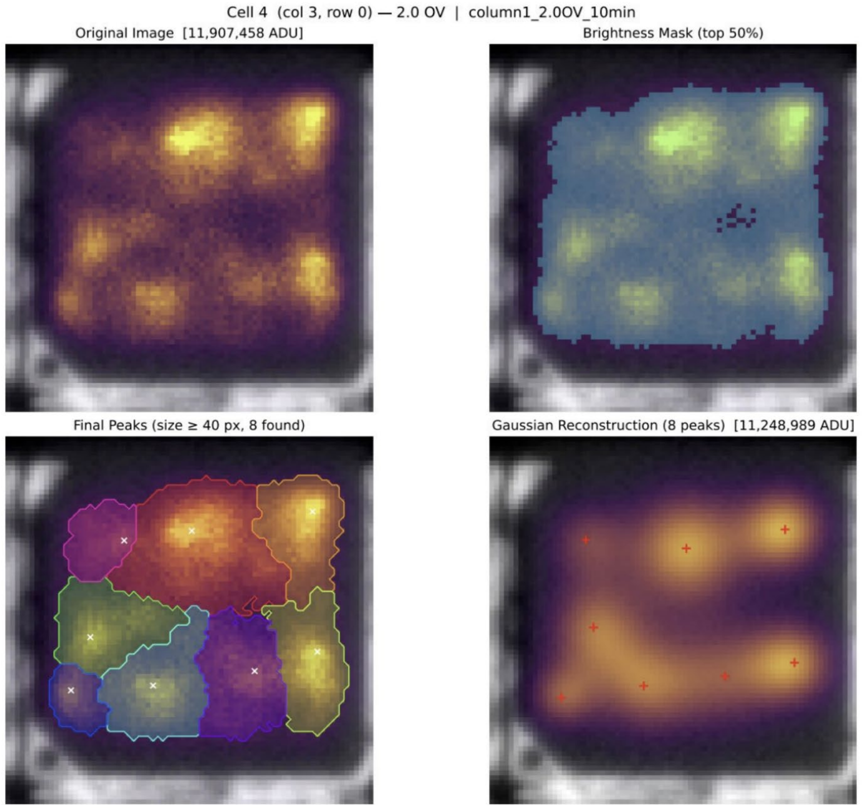

Threshold → peaks → watershed → 2D Gaussians

EMG Parameters: Hotspot Intensity (FBK)

Table 4: Extracted EMG fit parameters (μ, σ, λ) and most probable value (MPV) of the hotspot *intensity* for the FBK sensor across the four irradiated fluences and their measured overvoltages. Both the MPV and the peak position μ grow monotonically with overvoltage and with fluence, from an MPV of 3.50 at the lowest fluence and overvoltage to 41.52 at the highest, quantifying the trends plotted in Fig. 44.

Fluence	**OV (V)**	$\boldsymbol{\mu}$	$\boldsymbol{\sigma}$	$\boldsymbol{\lambda}$	**MPV**
3.0×10^{11} n_{eq}/cm^2	1.0	2.48	0.45	0.073	3.50
	2.0	5.15	1.07	0.025	7.68
	3.0	8.88	2.10	0.014	13.73
	4.0	13.11	3.37	0.010	20.78
1.0×10^{12} n_{eq}/cm^2	1.0	6.37	1.44	0.079	8.86
	1.6	11.36	2.72	0.040	16.12
	2.3	17.51	4.02	0.024	24.75
	3.0	25.86	6.80	0.018	37.43
3.0×10^{12} n_{eq}/cm^2	1.0	10.15	2.28	0.114	13.21
	1.5	15.97	3.38	0.062	20.84
	2.0	23.84	5.69	0.045	31.50
	2.5	31.33	7.24	0.035	41.15
1.0×10^{13} n_{eq}/cm^2	1.0	12.96	1.83	0.151	15.35
	1.4	20.06	3.64	0.111	24.15
	1.7	24.90	4.39	0.091	29.84
	2.0	29.83	5.20	0.077	35.67
	2.3	34.89	5.84	0.067	41.52

48

EMG Parameters: Size & Current (FBK)

EPFL

Table 5: Extracted EMG fit parameters (μ, σ, λ) and most probable value (MPV) of the hotspot *spatial size* (σ, in µm) for the FBK sensor across the four irradiated fluences and their overvoltages. The size MPV increases only gently, from 2.06 to 2.93 µm, over the full range, confirming that irradiation and overvoltage affect the hotspot brightness far more than its size (cf. Tab. 4).

Fluence	**OV (V)**	$\boldsymbol{\mu}$	$\boldsymbol{\sigma}$	$\boldsymbol{\lambda}$	**MPV**
3.0×10^{11} n_{eq}/cm^2	1.0	1.86	0.34	3.963	2.06
	2.0	2.07	0.27	3.318	2.27
	3.0	2.21	0.26	3.024	2.42
	4.0	2.34	0.29	3.002	2.56
1.0×10^{12} n_{eq}/cm^2	1.0	2.14	0.36	3.812	2.34
	1.6	2.24	0.32	3.545	2.45
	2.3	2.29	0.30	3.218	2.51
	3.0	2.35	0.31	3.159	2.57
3.0×10^{12} n_{eq}/cm^2	1.0	2.28	0.41	2.735	2.54
	1.5	2.36	0.36	2.589	2.62
	2.0	2.42	0.37	2.636	2.68
	2.5	2.45	0.37	2.487	2.72
1.0×10^{13} n_{eq}/cm^2	1.0	2.44	0.49	2.852	2.72
	1.4	2.42	0.44	2.361	2.73
	1.7	2.52	0.48	2.513	2.82
	2.0	2.56	0.48	2.375	2.87
	2.3	2.62	0.49	2.419	2.93

Table 6: Extracted EMG fit parameters (μ, σ, λ) and most probable value (MPV) of the per-hotspot *current contribution* (in nA) for the FBK sensor across the four irradiated fluences and their overvoltages. The MPV grows by more than an order of magnitude across the range studied, from 0.13 nA to 4.57 nA, combining the brightness and size trends of Tab. 4 and Tab. 5 into a single per-site measure of dark activity.

Fluence	**OV (V)**	$\boldsymbol{\mu}$	$\boldsymbol{\sigma}$	$\boldsymbol{\lambda}$	**MPV**
3.0×10^{11} n_{eq}/cm^2	1.0	0.09	0.01	0.433	0.13
	2.0	0.24	0.02	0.140	0.32
	3.0	0.50	0.12	0.073	0.84
	4.0	0.87	0.28	0.046	1.61
1.0×10^{12} n_{eq}/cm^2	1.0	0.33	0.08	0.321	0.52
	1.6	0.70	0.21	0.162	1.19
	2.3	1.23	0.32	0.097	1.96
	3.0	1.80	0.59	0.068	3.10
3.0×10^{12} n_{eq}/cm^2	1.0	0.63	0.16	0.298	0.96
	1.5	1.26	0.35	0.173	1.97
	2.0	1.83	0.58	0.117	2.96
	2.5	2.67	0.96	0.089	4.46
1.0×10^{13} n_{eq}/cm^2	1.0	1.02	0.23	0.280	1.48
	1.4	1.57	0.40	0.184	2.35
	1.7	2.03	0.52	0.144	3.03
	2.0	2.41	0.57	0.117	3.53
	2.3	3.07	0.78	0.098	4.57